International Journal of Hydrogen Energy

Direct Numerical Simulation of Turbulent Premixed Ammonia and Ammonia-Hydrogen Combustion Under Engine-Relevant Conditions

--Manuscript Draft--

Manuscript Number:	
Article Type:	Full Length Article
Section/Category:	Heat Engines / Combustion / Heat Transfer
Keywords:	Direct Numerical Simulation; Ammonia-Hydrogen Fuel Blends; Premixed Combustion; High Turbulence; Elevated Pressure; NO formation
Corresponding Author:	Ranga Dinesh University of Southampton Southampton, UNITED KINGDOM
First Author:	W Yang
Order of Authors:	W Yang
	Ranga Dinesh
	K.H Luo
	D Thevenin
Abstract:	The combustion characteristics of ammonia and ammonia-hydrogen fuel blends under spark-ignited turbulent premixed engine-relevant conditions were investigated by means of direct numerical simulation and detailed chemistry. Several test cases were investigated for an outwardly expanding turbulent premixed flame configuration covering pure ammonia and ammonia-hydrogen fuel blends with 10% and 15% hydrogen content by volume for different equivalence ratio values of 0.9, 1.0 and 1.1. The results showed that the fuel-lean flames exhibit strong wrinkled structures at flame front compared to stoichiometric and fuel-rich flames. The heat release rate plots indicate that adding hydrogen into ammonia improves the reactivity of the flame and enhances the combustion process. The scatter plots of heat release rate versus local curvature coloured by NO formation, show that high heat release rate values occur in the concave structures and low heat release rate values occur in the convex structure, which is consistent with NO distribution. The highest turbulent burning velocity values were found for the fuel-lean cases because of the more wrinkled flame front with lower effective Lewis number compared to fuel-rich cases. The results found a bending effect for the ratio between turbulent to laminar burning velocities with respect to hydrogen addition at all tested equivalence ratios with 10% hydrogen addition into ammonia exhibiting a peak value for the burning velocity ratio. Two distinct flame structures (concave and convex) were analysed in terms of local equivalence ratio based on the elements of N, O and H, O. They revealed an opposite distribution of NO formation normal to the flame front within concave and convex structures. Elementary chemical reactions involved in NO formation have shown that hydrogen addition into ammonia influences the reactivity of certain chemical reactions.

Dr. K. K. J. Ranga Dinesh
Lecturer in Energy Technologies Energy Technology Research Group
University of Southampton, Southampton, SO17 1BJ, UK.

Dear Editor,

Please find enclosed the paper, titled “Direct numerical simulation of turbulent premixed ammonia and ammonia-hydrogen combustion under engine relevant conditions” by W. Yang, K.K.J. Ranga Dinesh, K.H. Luo and D. Thevenin. This paper is an original research paper based on the work carried out by the first author leading to investigate combustion characteristics of turbulent premixed ammonia and ammonia-hydrogen fuel blends and it has not been submitted to other journals.

Sincerely,
K.K.J. Ranga Dinesh
December 2021

Suggested Reviewers

1.Prof. Xi Jiang,
School of Engineering and Material Science, Queen Mary University London, UK
Email: xi.jiang@qmul.ac.uk

2. Dr. Oliver Stein, Deputy Director,
Institute for Combustion Technology
University of Stuttgart
Germany.
Email: o.stein@itv.uni-stuttgart.de

3. Prof. Karl Jenkins,
Centre for Computational Engineering Sciences, School of Engineering, Cranfield University, UK.
Email: k.w.jenkins@cranfield.ac.uk

Highlights

- DNS study of premixed ammonia and ammonia-hydrogen combustion.
- Adding hydrogen into ammonia improves the reactivity of the flame.
- 10% hydrogen addition by volume into ammonia provides better flame conditions.
- NO formation at concave and convex structures are analysed.

Direct Numerical Simulation of Turbulent Premixed Ammonia and Ammonia-Hydrogen Combustion Under Engine-Relevant Conditions

W. Yang[1], K.K.J. Ranga Dinesh[2*], K.H. Luo[3], D. Thevenin[4]

1. Center for Combustion Energy, Department of Energy and Power Engineering, Tsinghua University, 10084, Beijing, China.

2. Energy Technology Research group, School of Engineering, Faculty of Engineering and Physical Sciences, University of Southampton, Southampton, SO17 1BJ, UK.

3. Department of Mechanical Engineering, University College London, Torrington Place, London WC1E 7JE, UK.

4. Laboratory of Fluid Dynamics and Technical Flows, University of Magdeburg "Otto von Guericke", Universitatsplatz 2, D-39106 Magdeburg, Germany.

Corresponding author email address: dinesh.kahanda-koralage@soton.ac.uk

Telephone: +44 (0)23 8059 2872

Manuscript prepared for the submission of International Journal of Hydrogen Energy

Abstract

The combustion characteristics of ammonia and ammonia-hydrogen fuel blends under spark-ignited turbulent premixed engine-relevant conditions were investigated by means of direct numerical simulation and detailed chemistry. Several test cases were investigated for an outwardly expanding turbulent premixed flame configuration covering pure ammonia and ammonia-hydrogen fuel blends with 10% and 15% hydrogen content by volume for different equivalence ratio values of 0.9, 1.0 and 1.1. The results showed that the fuel-lean flames exhibit strong wrinkled structures at flame front compared to stoichiometric and fuel-rich flames. The heat release rate plots indicate that adding hydrogen into ammonia improves the reactivity of the flame and enhances the combustion process. The scatter plots of heat release rate versus local curvature coloured by NO formation, show that high heat release rate values occur in the concave structures and low heat release rate values occur in the convex structure, which is consistent with NO distribution. The highest turbulent burning velocity values were found for the fuel-lean cases because of the more wrinkled flame front with lower effective Lewis number compared to fuel-rich cases. The results found a bending effect for the ratio between turbulent to laminar burning velocities with respect to hydrogen addition at all tested equivalence ratios with 10% hydrogen addition into ammonia exhibiting a peak value for the burning velocity ratio. Two distinct flame structures (concave and convex) were analysed in terms of local equivalence ratio based on the elements of N, O and H, O. They revealed an opposite distribution of NO formation normal to the flame front within concave and convex structures. Elementary chemical reactions involved in NO formation have shown that hydrogen addition into ammonia influences the reactivity of certain chemical reactions.

Key Words: Direct Numerical Simulation, Ammonia-Hydrogen Fuel Blends, Premixed Combustion, High Turbulence, Elevated Pressure, NO formation

1.Introduction

With the increasing threat of climate change on earth, it is necessary to utilise low carbon and clean fuel options to reduce greenhouse gas emissions and regulated pollutant emissions from combustion engines. Searching for alternative fuels with zero-carbon combustion emissions such as in hydrogen (H_2) and ammonia (NH_3) is becoming more popular in recent combustion research for a range of combustion devices such as internal combustion engines, gas turbines and burners.

Hydrogen has been widely recognised as a clean fuel for decades and the combustion characteristics of hydrogen is generally well-known. Nevertheless, there are still unsolved challenges in large-scale utilisation of hydrogen fuel in combustion devices such as internal combustion engines and gas turbine engines, because of issues in hydrogen supply chain, economic storage and secure transport [1]. Recently, ammonia has emerged as a promising zero-carbon fuel and hydrogen-energy-carrier due to its very high hydrogen content and easy liquefaction by compression compared to hydrogen. For example, ammonia can be stored in liquid form at 9.9 atm and room temperature (25°C) or at 1 atm and temperature of -33.4°C [1,2]. There is a clear advantage for ammonia over hydrogen when it comes to economic storage and secure transport. However, ammonia is a low reactive zero-carbon fuel and it faces different challenges for its utilisation in combustion engines. For example, combustion characteristics of ammonia fuel exhibits low combustion intensity, low burning velocity and high nitric oxide (NOx) emissions compared to combustion characteristics of hydrogen fuel. The ammonia fuel also has high auto-ignition temperature and low flammability range compared to hydrogen fuel. The most common methods of enhancing combustion intensity of ammonia-air are hydrogen addition and oxygen-enrichment.

In recent years, various fundamental and applied research studies have been carried out to address the chemical kinetics and burning characteristics of ammonia, ammonia-hydrogen fuel blends and ammonia-methane fuel blends under laminar and turbulent flow conditions at atmospheric and elevated pressures. For example, detailed and/or reduced chemical mechanisms have been developed for pure ammonia combustion [3-12], ammonia-hydrogen and ammonia-methane fuel blends [13-23]. Most of the studies on detailed chemical kinetics have considered more than 100 elementary reactions [4-6, 17]. Several studies have applied reduced chemical kinetic mechanisms for ammonia combustion. For example, Duynslaegher et al. [8,10] studied a flat, freely propagating flame of premixed ammonia-air flames under various spark-ignition engine operation conditions (1-49 atm., 295-732 K), which showed the peak laminar burning velocity at equivalence ratio of 1.12 while the highest adiabatic flame temperature occurred at stoichiometric condition. Xiao et al. [14-15] have tested the applicability of reduced chemistry mechanisms developed by Tian [6] and Mathieu [11] for ammonia-hydrogen combustion under practical engine conditions, and found good agreement with the experimental data for laminar burning velocity and ignition delay time. Rocha et al. [20] developed three reduced chemistry mechanisms, consisting of less than 80 reactions, which have been validated by Cantera in terms of shock tube ignition delay times, laminar burning velocity and NOx emissions for ammonia-air and ammonia-hydrogen-air mixtures as a function of equivalence ratio at elevated pressure and different temperature conditions. They found that pure ammonia flames exhibit high ignition delay times and lower burning velocity, while the mixture of ammonia-hydrogen can improve the combustion behaviour of ammonia flame. Shrestha et al. [21] studied a reduced chemistry mechanism for ammonia-hydrogen fuel blends with oxygen-enriched conditions at intermediate temperature and elevated pressure. They found that 9% increase of oxygen by mass compared to air has the same effect as 30% hydrogen addition by mass in ammonia-hydrogen fuel blend.

Besides the above noted studies on chemical kinetic mechanisms for ammonia and ammonia fuel blends, there is a body of literature on experimental and numerical investigations of ammonia and ammonia fuel blends at atmospheric and high pressure conditions [24-48]. Lee et al. [25] have carried out an experimental study of spark-ignited spherical laminar premixed ammonia/hydrogen/air flames and found that preferential-diffusional and hydrodynamic cellular instabilities in hydrogen-air combustion can be suppressed by ammonia addition instead of methane, especially under for fuel-lean conditions. Hayakawa et al. [27] have experimentally clarified the decreasing unstretched laminar burning velocity of ammonia/air laminar premixed flames with the pressure increase. They also found that the Markstein length increases with an increase in equivalence ratio. Meanwhile, Okafor [32] calculated the laminar burning velocity and Markstein length of ammonia-methane-air laminar flames with pressures up to 0.50MPa, which revealed that more ammonia in the fuel and high pressure led to lower unstretched laminar burning velocity. At high pressures, the Markstein length decreased with an increase of ammonia for the lean flame, and opposite tendency was observed for the rich flame. Furthermore, Lhuillier et al. [34] obtained data for laminar burning velocity of premixed ammonia-hydrogen-air flames at atmospheric pressure and intermediate temperature with hydrogen addition up to 60% by volume. They found that laminar burning velocities increase with increasing hydrogen fraction and unburned gas temperature.

Several experimental and numerical studies were conducted to study ammonia and ammonia fuel blends under turbulent conditions [36-48]. The experimental study of Ichikawa et al. [41] have revealed that the ratio of the turbulent burning velocity and unstretched laminar burning velocity decreased with an increase in the ammonia content in ammonia-methane-air mixtures at 0.5 MPa. The experimental study of Ichimura et al. [42] have determined the extinction limits

of ammonia/air flames in turbulent fields based on parameters such as Karlovitz number and Markstein number. Xia et al. [47] have concluded that under oxygen-enriched air condition, the effects of diffusional–thermal instability and turbulence are important to turbulent flame propagation velocity in ammonia combustion fields and the ratio of turbulent to laminar burning velocity increased with turbulence Karlovitz number. Lhuillier et al. [46] have carried out experimental work on ammonia combustion behaviour in a spark ignition engine by means of expanding flames, covering a wide range of conditions such as equivalence ratio (0.8 to 1.4), hydrogen addition (0 to 60% by volume), initial temperature (298 to 473 K) and pressure (0.1, 0.54 MPa). They have reported an unexpected bending effect for the turbulent-to-laminar velocity ratio at certain equivalence ratios with respect to increased hydrogen fraction in ammonia-hydrogen fuel blends. Okafor et al. [44,45] performed large eddy simulation (LES) studies of bluff body stabilised turbulent non-premixed ammonia-air swirling flames and analysed NOx emissions for a wide range of equivalence ratios.

Based on the literature, there is a research gap in a detailed and fully resolved numerical investigation of ammonia and ammonia fuel blends under engine-relevant conditions. Direct numerical simulation (DNS) of turbulent combustion [49,50] has been very effective in the investigation of fundamental flame characteristics and turbulence-chemistry interaction of classical hydrocarbon fuels and emerging clean fuels such as ammonia. A large number of DNS studies have been performed to investigate fundamental combustion characteristics of alternative and clean fuels such as hydrogen [51-54], syngas [55-57] and Dimethyl Ether (DME) [58]. With respect to ammonia, the two-dimensional DNS of wrinkled laminar premixed flames under atmospheric condition was conducted by Netzer et al. [59], showing relationship between flame curvature and NO formation. They also found that NO formation

is affected by thermo-diffusive process with respect to hydrogen addition including two competing pathways of decomposition of amino radical.

In the present study, fundamental flame characteristics of turbulent premixed ammonia and ammonia-hydrogen fuel blends under spark ignition engine-relevant conditions is studied by means of two-dimensional direct numerical simulation and detailed chemistry. We employed a centrally-ignited outwardly propagating turbulent premixed spherical flame configuration. We study fundamental combustion characteristics such as flame front propagation, burning velocities, heat release rate, flame curvature and NO formation of turbulent premixed pure ammonia flame and ammonia-hydrogen blended flames at three different equivalence ratios (lean, stoichiometric and rich conditions) under high turbulence intensity and elevated pressures. The remaining sections will discuss mathematical modelling and numerical computation, results and discussion, and summary of key conclusions.

2. Mathematical Modelling and Numerical Computation

To investigate the combustion characteristics of ammonia and ammonia-hydrogen fuel blends, the parallel DNS code, PARCOMB [55-57] [60] is used. The DNS code solved fully compressible unsteady governing equations for mass, momentum, total internal energy, mass fraction of species concentration as well as equation of state on a uniform two-dimensional Cartesian grid [55]. The diffusive process of the species transport equation is calculated using the mixture-averaged transport model supplemented with a model for Soret effect (thermal diffusion). The spatial derivatives are computed using the six order cell centred explicit scheme and the order is progressively reduced to four at boundaries. The time integration is carried out with a fourth-order Runge-Kutta scheme. A Courant–Friedrichs–Levy (CFL) condition for the convective terms and a Fourier condition pertaining to the diffusion terms are treated to ensure

the stability of the explicit integration and determine a suitable time step. The boundary conditions are treated with Navier-Stokes characteristics boundary conditions (NSCBC) with modified pressure relaxation treatment [55-57] to maintain a constant pressure throughout the simulations. The initial homogeneous isotropic turbulent velocity field is implemented by using a combined approach of digital filtering and random noise diffusion [55-57].

A centrally-ignited outwardly propagating (expanding spherical) flame with high turbulence level and elevated pressure is applied for the present investigation. Nine different two-dimensional DNS test cases of ammonia and ammonia-hydrogen fuel blends under spark-ignited initial temperature of 445 and initial pressure of 0.54MPa are simulated. The simulations are carried out for three different equivalence ratios, 0.9, 1.0 and 1.1. The ammonia-hydrogen fuel blends are simulated for 10% and 15% hydrogen blends by volume, respectively. The test cases including fuel mixtures, equivalence ratio, initial turbulent properties and pressure are selected from a recently carried out experimental study of ammonia combustion behaviour in spark-ignited turbulent expanding flames [46]. The test cases and parameters are listed in Table 1.

Table 1: Turbulent properties and parameters for all simulations.

Fuel	ϕ	u'(m/s)	lt(mm)	Ret[a]	Grid	Cell width(μm)	η(μm)[b]	Da[c]	Ka[d]	Le_{eff}
Pure NH_3	0.9	1.0	3.4	583.4	2501^2	8	28.64	0.34	70.80	0.98
Pure NH_3	1.0	1.0	3.4	583.4	2501^2	8	28.64	0.52	46.27	1.00
Pure NH_3	1.1	1.0	3.4	583.4	2501^2	8	28.64	0.64	37.50	1.05
90% NH_3 10% H_2	0.9	1.0	3.4	580.2	2501^2	8	28.76	0.57	42.03	0.96
90% NH_3 10% H_2	1.0	1.0	3.4	580.1	2501^2	8	28.76	0.85	28.40	1.00
90% NH_3 10% H_2	1.1	1.0	3.4	579.7	2501^2	8	28.78	1.05	22.93	1.04
85% NH_3 15% H_2	0.9	1.0	3.4	578.7	2501^2	8	28.82	0.75	31.91	0.95
85% NH_3 15% H_2	1.0	1.0	3.4	578.1	2501^2	8	28.84	1.10	21.89	1.00
85% NH_3 15% H_2	1.1	1.0	3.4	577.7	2501^2	8	28.85	1.35	17.76	1.03

u'-Root-mean-square (RMS) turbulent fluctuation velocity.

l_t-Integral length scale measured directly from the initial turbulence field.

λ-Taylor length scale, $\lambda = l_t Re_t^{-0.5}$

S_L-Laminar burning velocity.

δ_L-Laminar flame thickness, $\delta_L = (T_b - T_u)/(\max|\nabla T|)$.

λ-Taylor length scale, $\lambda = l_t Re_t^{-0.5}$.

a-Turbulent Reynolds number, $Re_t = u' l_t/\nu$.

b-Kolmogorov length scale, $\eta = l_t Re_t^{-0.75}$.

c-Damköhler number, $Da = (l_t/\delta_L)(S_L/u')$.

d-Karlovitz number, $Ka = (\delta_L/\lambda)(u'/S_L)$.

The chemical mechanism with 21 species and 49 elementary reactions based on Rocha et al. [20] is implemented. The simulations are performed for a 2 cm square domain using uniform Cartesian grid with 2501 x 2501 grid points with grid resolution of 8 μm. The approximate time step is 4.5 ns. Both resolution and time step in the present DNS study are appropriate under 0.54MPa compared to reference [59], in which they have carried out DNS calculations with resolution of 20 μm and time step of 5 ns under 0.1MPa, combined with 19 species and 60 elementary reactions. In the present DNS study, the resolution is 3~4 times smaller than the Kolmogorov scale of 28 μm. This suggests that we have fully resolved the flame thickness in our DNS test cases where simulated flames develop under high turbulence and elevated pressure. As shown in Fig. 1, the initial spherical laminar flame kernel (red area) is placed at the centre of the computational domain with radius of r_0 = 0.2 cm and the fresh gas mixture (blue area) is filled in the rest of the computational domain. The initial profiles of temperature and mass fractions of species are described according to:

$$\phi=\phi_0+\frac{\Delta\phi}{2}\left[1\text{-}\tanh\left(k\left(\frac{r\text{-}r_0}{r_0}\right)\right)\right] \quad (1)$$

where $\Delta\phi$ is the variation between the initial values in the fresh and burnt gas mixture and the measurement of stiffness is number k, which is set to the value of 10 in this study.

All nine cases are in the thin reaction zones in the Peters-Borghi's diagram, which can be seen in Fig. 2.

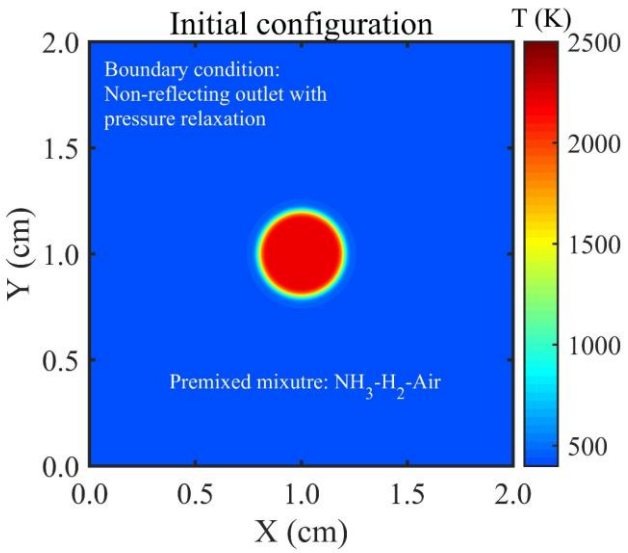

Fig. 1 Initial temperature configuration: fresh gas (blue) and burnt gas (red).

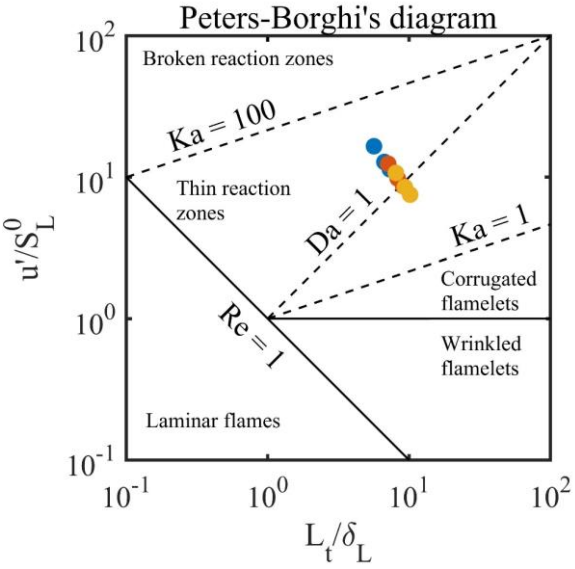

Fig. 2 Peters-Borghi's diagram showing simulated test cases (blue dots: pure NH_3, red dots: 90% NH_3-10% H_2 by volume, yellow dots: 85% NH_3-15% H_2 by volume.

Several parameters are used to analyse the DNS data. The effective Lewis number [57] is defined as the combination of the fuel and oxidizer:

$$Le_{eff}= \frac{Le_D+ALe_E}{1+A},\ A= \begin{cases} 1+\beta\left(\phi^{-1}-1\right) & \phi<1 \\ 1+\beta(\phi-1) & \phi>1 \end{cases} \quad (2)$$

where Le_D and Le_E are the Lewis number of deficient and excessive reactants, respectively. And the Lewis number of ammonia-hydrogen is:

$$Le_{NH_3/H_2}=1+ \frac{q_{NH_3}\left(Le_{NH_3}-1\right)+q_{H_2}\left(Le_{H_2}-1\right)}{q_{NH_3}+q_{H_2}}, \quad q_i= \frac{QY_i}{C_pT_u} \quad (3)$$

where q_i is the non-dimensional heat release associated with the consumption of species i, which refers to NH_3 and H_2. Q is the heat of reaction and Y_i is the mass fraction [57].

The local heat release rate is calculated by the following equation:

$$Q = \sum_{k=1}^{N_s} h_k\dot{\omega}_k \quad (4)$$

Non-dimensional progress variable based on temperature is derived to indicate the local chemical state between fresh gas mixture and fully burnt gases:

$$C = \frac{T-T_u}{T_b-T_u}=\begin{cases} 0 & \text{fresh gas mixture} \\ 1 & \text{fully burnt gases} \end{cases} \quad (5)$$

where T_u and T_b are the unburned and burned gas temperatures, respectively.

The local curvature is calculated from the flame front coordinates is calculated by:

$$\kappa = \left.\frac{\partial N_i}{\partial x_i}\right|_{c=c^*} \quad (6)$$

where κ is positive (negative) when the flame is convex (concave) in the direction of the unburned mixture. N_i is the ith component of the local flame normal vector, which uses the following formula:

$$N_i = -\frac{1}{|\nabla c|}\frac{\partial c}{\partial x_i} \quad (7)$$

3. Results and Discussion

In this section, we discuss fundamental turbulent premixed flame characteristics of ammonia and ammonia-hydrogen fuel blends under high turbulence and elevated pressure covering nine different test cases. All simulated test cases are listed in Table 1. We discuss flame propagation and burning characteristics of ammonia and ammonia-hydrogen fuel blends by analysing local flame curvature, heat release rate, NO distribution and burning velocities.

Spherical flame propagation and heat release rate

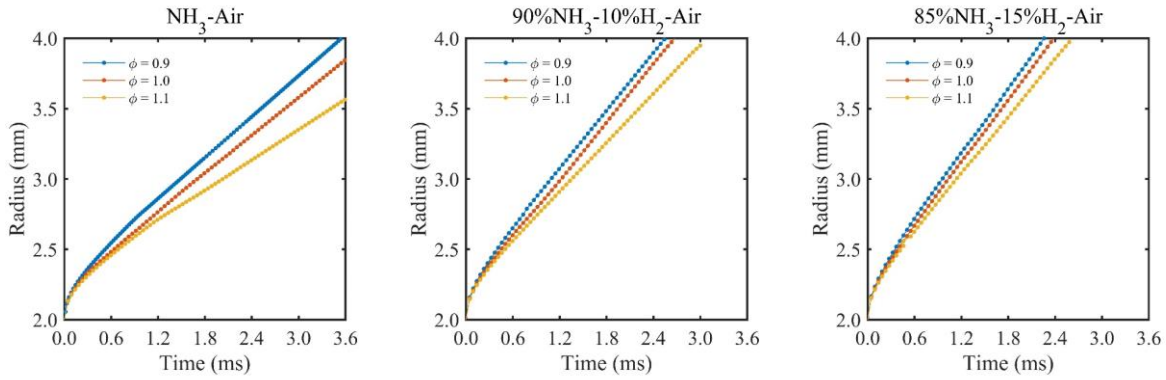

Fig.3. Mean flame radius as a function of time for ammonia and ammonia-hydrogen fuel blends at three different equivalence ratios.

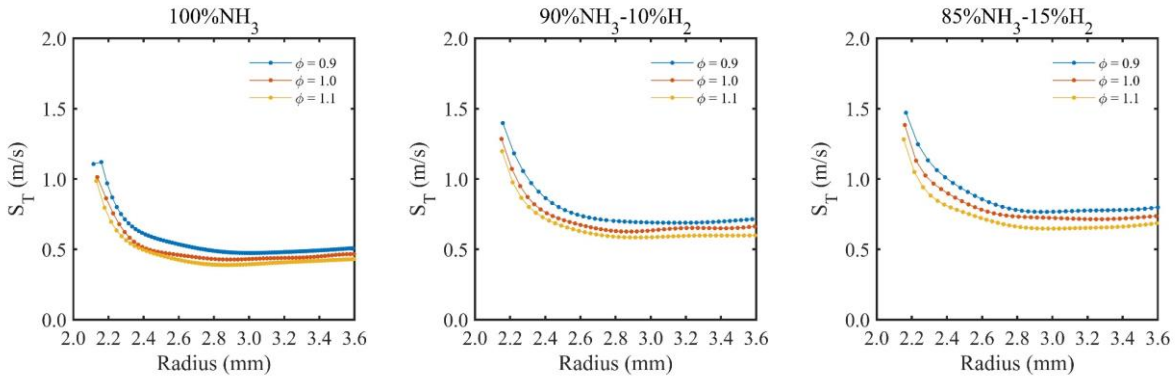

Fig. 4. Turbulent burning velocity as a function of mean flame radius for all test cases.

Fig. 3 illustrates the flame mean radius as a function of physical simulation time for ammonia and ammonia-hydrogen fuel blends at three different equivalence ratios. The peak heat release rate is located at C=0.5 which is considered as the flame front. The mean flame radius is

calculated based on the mean value of instantaneous flame front at C=0.5. In the present analysis, the pre-heat region is considered for C ≤0.1. the reaction layer is selected within a range of 0.4 ≤ C ≤0.6, and the fully burned region is considered for C > 0.6. The peak heat release rate is located at C=0.5 which is considered as the flame front.

It is seen that the initial laminar flame kernel influences the flame propagation at the beginning, where there is an apparent curve in the flame radius evolvement. The duration at the beginning stage affected by the initial kernel is within 0.5 ms for all cases. Beyond the kernel influenced period, the flame radius increases with respect to hydrogen addition into ammonia for ammonia-hydrogen cases under the same elapsed time for the same equivalence ratio. This observation demonstrates improved reactivity of the flame as a result of hydrogen addition into ammonia for ammonia-hydrogen fuel blends. Fig. 3 also shows that the flame radius grows more quickly for 15% hydrogen addition case compared to 10% hydrogen addition case. The lean condition displays the high flame radius for ammonia and ammonia-hydrogen blends, indicating possible higher turbulent burning velocity values compared to stoichiometric and rich conditions. Based on the mean flame radius, the turbulent burning velocity is calculated by $S_T = dR/dt$, where R is the radius and t is physical time. Fig. 4 shows the turbulent burning velocity as a function of mean radius for all test cases. It can be seen that the turbulent burning velocity values reduced at the beginning and then they become stable and flattened when the mean flame radius reaches around 3.0mm. This observation indicates that the simulated DNS spherical flames become fully developed when the mean flame radius reaches around 3.0mm. It is important to note that the changing trends of turbulent burning velocity values in our DNS results are consistent with the experimental study of [47]. The higher values of turbulent burning velocity are observed for ammonia-hydrogen fuel blends compared to pure ammonia which indicate that the combustion intensity of ammonia is explicitly enhanced by hydrogen.

For ammonia and ammonia-hydrogen flames, the fuel lean case exhibits the highest turbulent burning velocity value compared to stoichiometric and rich cases. In the following sections, the DNS data were gathered when each flame reaches the mean flame radius of R=3.5mm. We also gathered DNS data for each flame when the mean flame radius reaches R=3.0mm. The DNS data at two different mean flame radius values of R=3.5mm and R=3.0mm were analysed to ensure the validity of our calculation at different time instants.

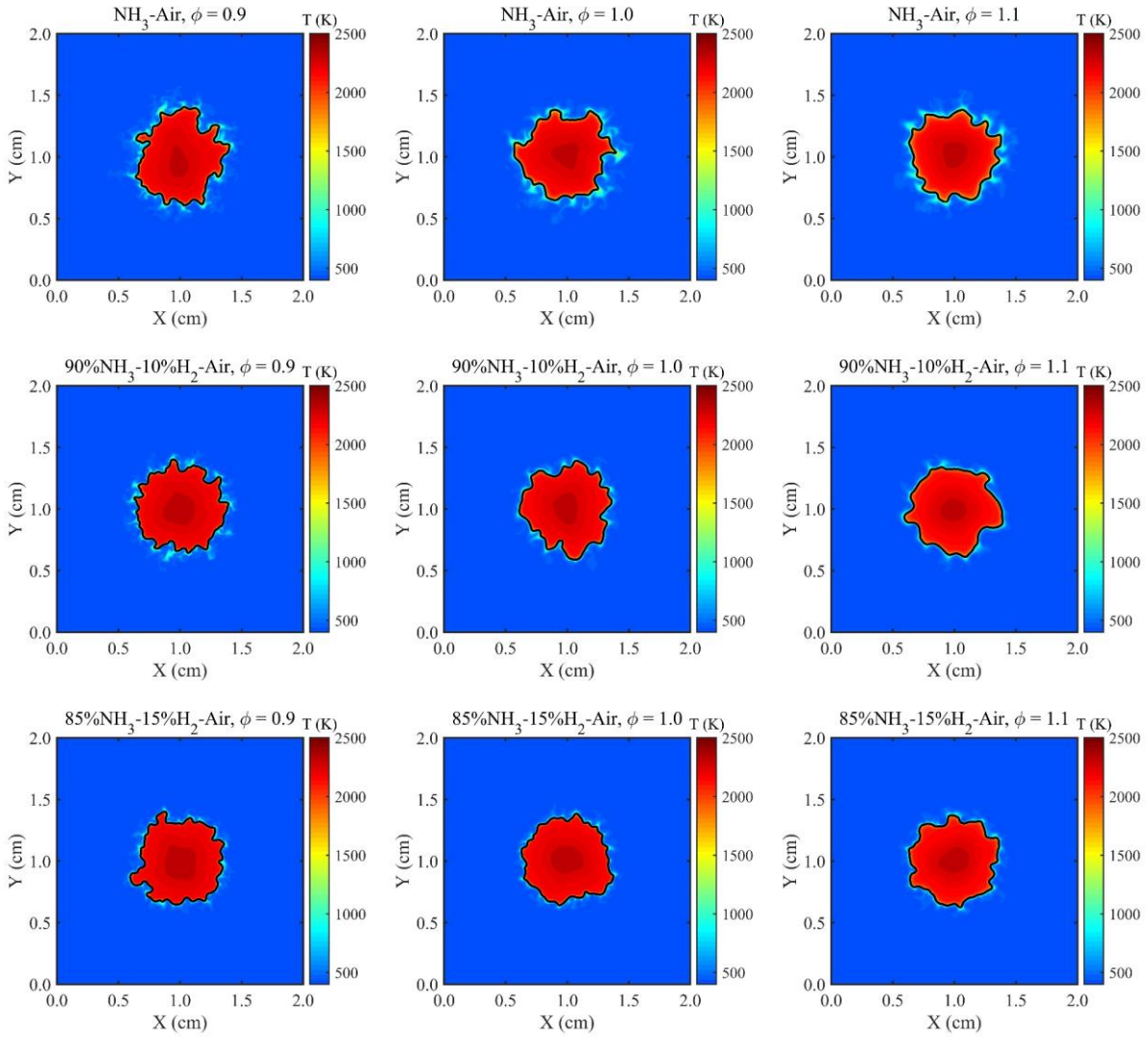

Fig. 5. Contour plots of flame temperature for all test cases at R = 3.5 mm.

Fig. 5 shows the flame front (black line around the red kernel) for all cases when the flame surface area is fixed corresponding to the mean flame radius of 3.5 mm. Fig. 5 shows roughly that the flame front undergoes less wrinkled structures when equivalence ratio changes from 0.9 to 1.1 for the same fuel type. Generally, less wrinkled structures are observed for the rich condition than the lean condition. However, it has been observed that blending hydrogen with ammonia (10% and 15% by volume) does not make any significant changes to flame front wrinkling structures for a given equivalence ratio.

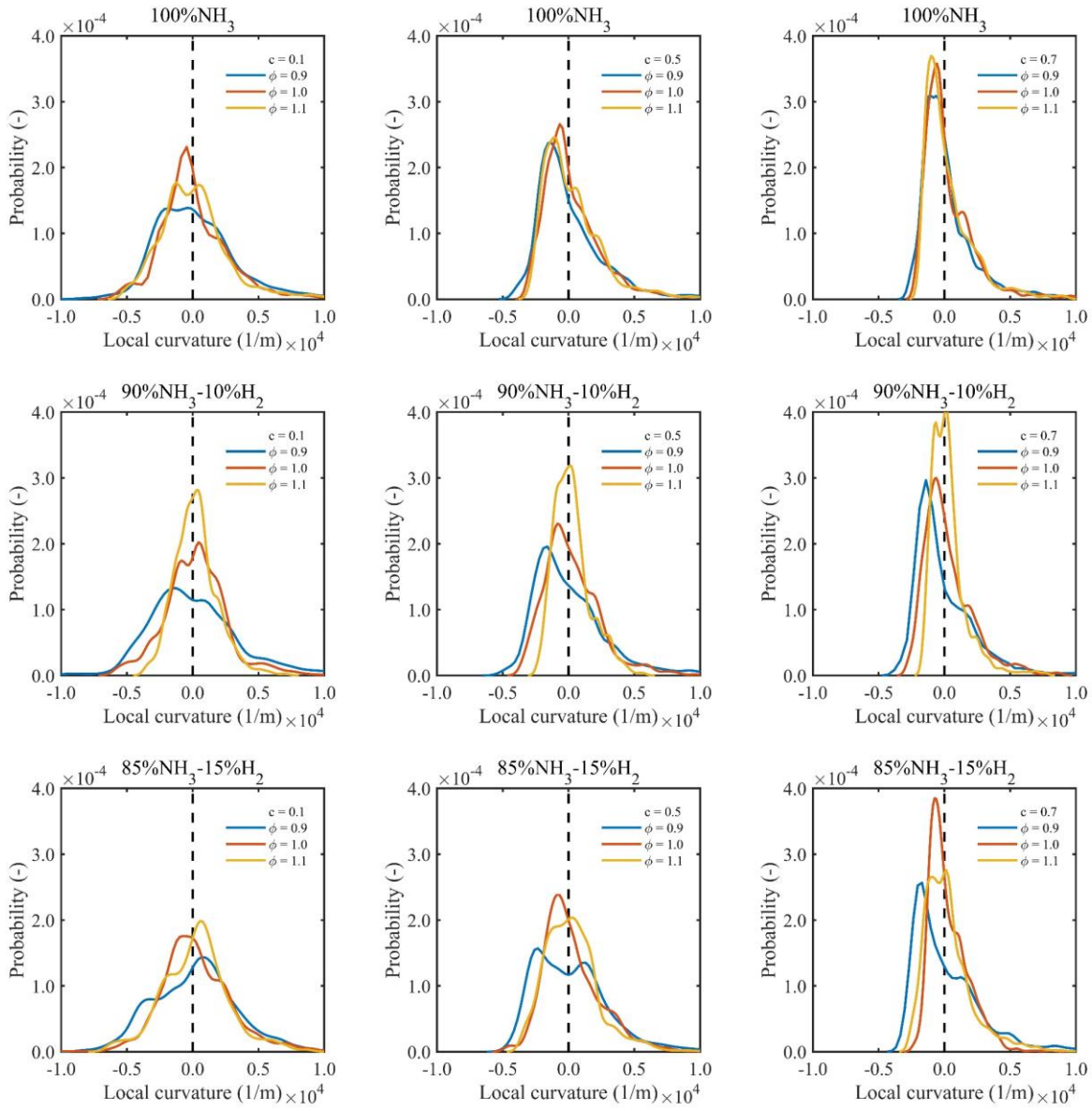

Fig. 6. Probability density functions of local curvature at pre-heat zone (C=0.1), reaction zone (C = 0.5), burned zone (C = 0.7) at mean flame radius, R = 3.5 mm.

The flame front behaviour can be further clarified by analysing the probability density functions (pdfs) of local flame curvature. For this, we have analysed pdfs of local curvature at pre-heat zone (C=0.1), reaction zone (C=0.5) and fully burned zone (C=0.7) when each flame developed up to the mean flame radius of R=3.5mm, see Fig.6. The peak value of probability is located very close to the local curvature of 0.0, at which the apex of probability undergoes the increment from lean to rich and preheat zone to burned region, respectively.

For stoichiometric and rich conditions, the width of the distribution of the local curvature for ammonia and ammonia-hydrogen flames are practically the same. However, the simulated flames under fuel lean condition perform slightly differently, which show the lower peak values of pdfs and wider boundaries than that observed for the stoichiometric and rich flames. Generally, Fig. 6 shows the distribution intensity of the local curvature centred at value of 0.0 for all simulated cases, indicating that much wider distribution range is corresponding to large number of flame convex (positive curvature) and concave (negative curvature) structures. The convex and concave structures promote the flame area growth and hence the turbulent burning velocity.

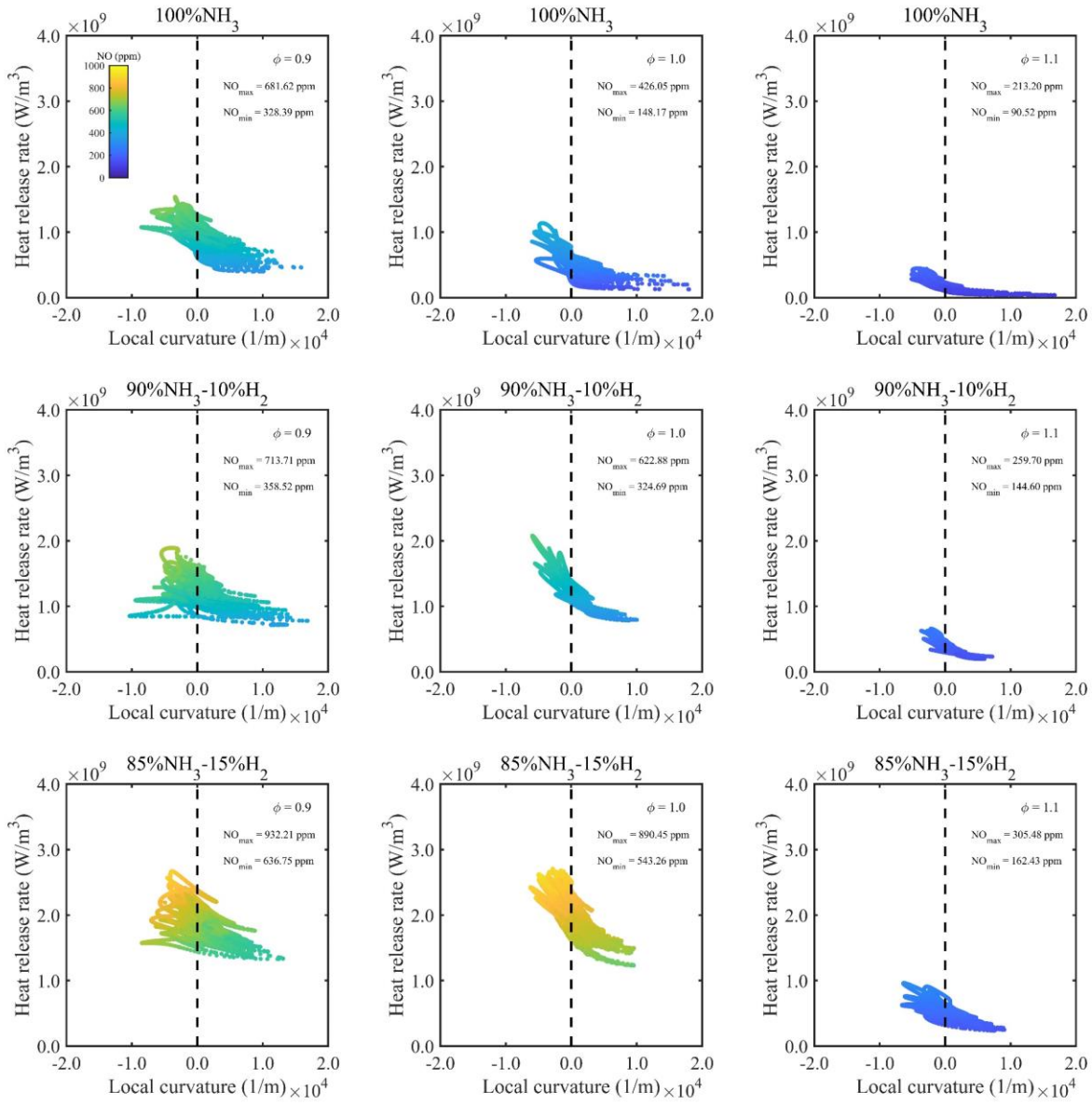

Fig. 7. Scatter plot of heat release rate versus local curvature at pre-heat zone (C=0.1) coloured by NO production at mean flame radius, R = 3.5 mm.

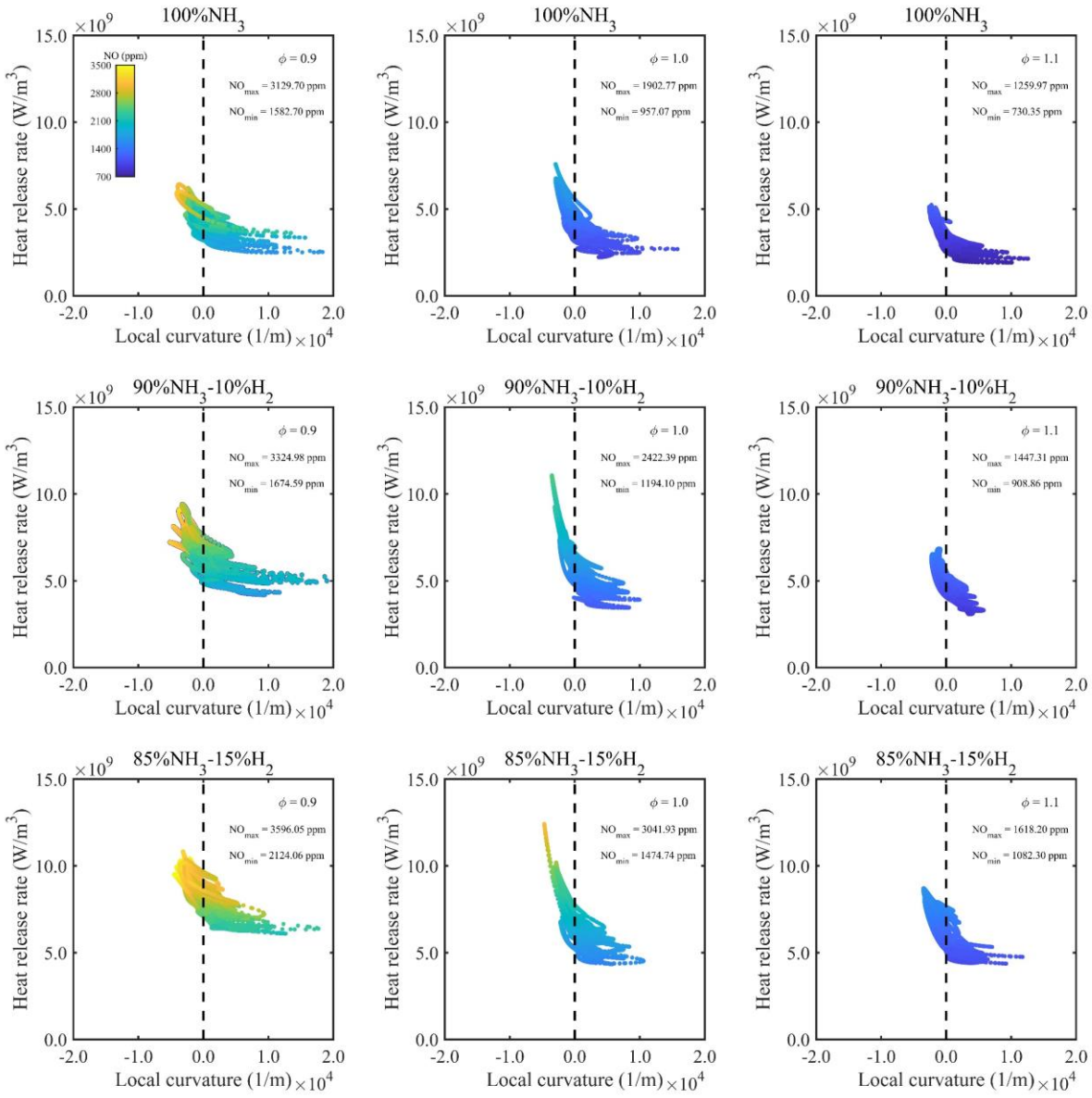

Fig. 8. Scatter plot of heat release rate versus local curvature at reaction zone (C=0.5) coloured by NO production at mean flame radius, R = 3.5 mm.

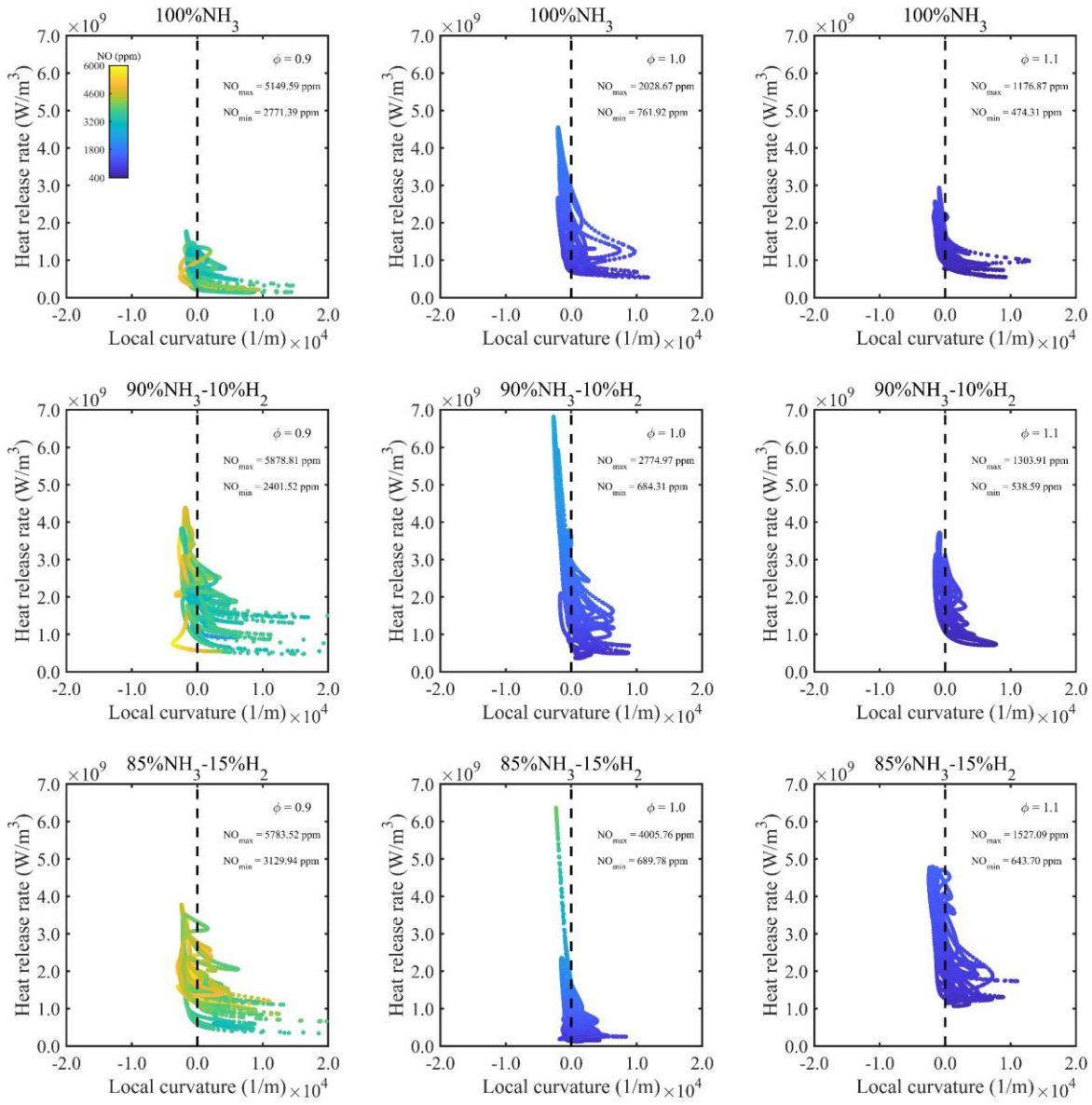

Fig. 9. Scatter plot of heat release rate versus local curvature at fully burned zone (C=0.7) coloured by NO production at mean flame radius, R = 3.5 mm.

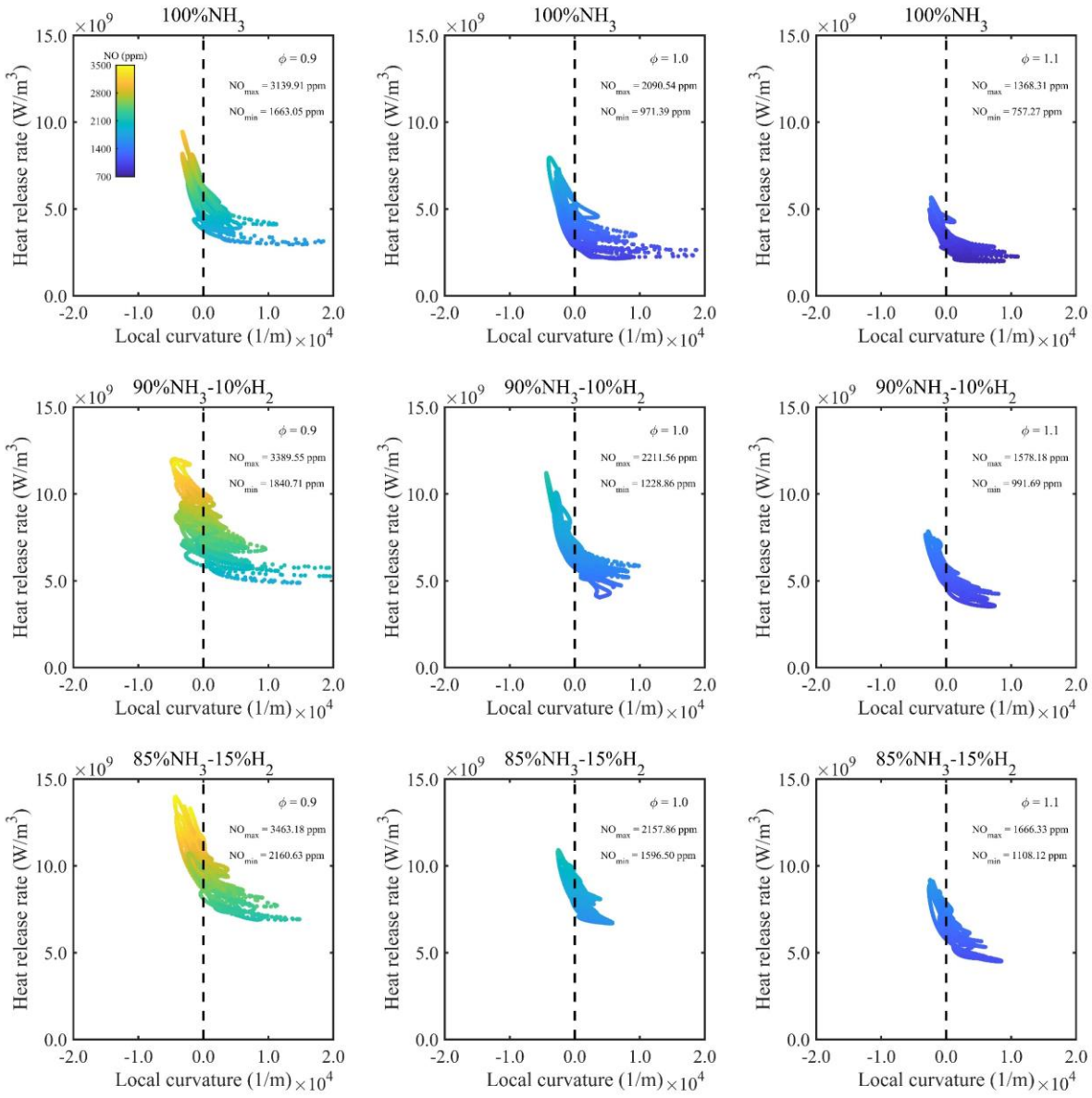

Fig. 10. Scatter plot of heat release rate versus local curvature at reaction zone (C=0.5) coloured by NO production at mean flame radius, R = 3.0 mm.

Figs. 7-9 illustrate the relationship between the local curvature and heat release rate coloured by NO formation at pre-heat zone (C = 0.1), reaction zone (C = 0.5) and fully burned zone (C=0.7) and at mean flame radius, R=3.5 mm. All three figures illustrate that the higher heat release rate values occur in the concave regions while the lower values are in the convex regions. With hydrogen addition into ammonia, the whole area of heat release rate is increasing, indicating more hydrogen burning is taking place in the combustion of ammonia-hydrogen fuel blends. We also observed the shift from pre-heat zone to fully burned zone, causing the transition of heat release rate distribution from negative local curvature region (concave structures) to more steep scattering with more points around zero curvature. The NO formation mainly occurs in the higher heat release zone and NO values change when the fuel-oxidizer mixture varies from pre-heat zone to fully burned zone.

To compare the results between two different time instants, we also plotted scatter plots of heat release rate versus local curvature at reaction zone (C=0.5) and at mean flame radius, R=3.0 mm. As seen in Fig. 10, the scatter plots of heat release rate versus local curvature at reaction zone (C=0.5) and at mean flame radius, R=3.0 mm shows nearly the same shape and distribution region compared with Fig. 8. Even the maximum and minimum NO values are nearly the same at two mean flame radius values of R=3.0 mm and R=3.5 mm, which are tabulated in Table 2 and 3 and the same trends are also reported in [59]. The steady state NO values calculated at two mean flame radius values of R=3.0 mm and R=3.5 mm further confirms that the simulated flames were fully developed when each flame reaches the mean flame radius value of R=3.0 mm.

R = 3.0 mm C = 0.5	ϕ = 0.9	ϕ = 1.0	ϕ = 1.1
100% NH3	3139 1663	2090 971	1368 757
90% NH3 10% H2	3389 1840	2211 1228	1578 991
85% NH3 15% H2	3463 2160	2157 1596	1666 1108

Table 2: Maximum and minimum values of NO formation (ppm) at R = 3.0 mm.

R = 3.5 mm C = 0.5	ϕ = 0.9	ϕ = 1.0	ϕ = 1.1
100% NH3	3129 1582	1902 957	1259 730
90% NH3 10% H2	3324 1674	2422 1194	1447 908
85% NH3 15% H2	3596 2124	3041 1474	1618 1082

Table 3: Maximum and minimum values of NO formation (ppm) at R = 3.5 mm.

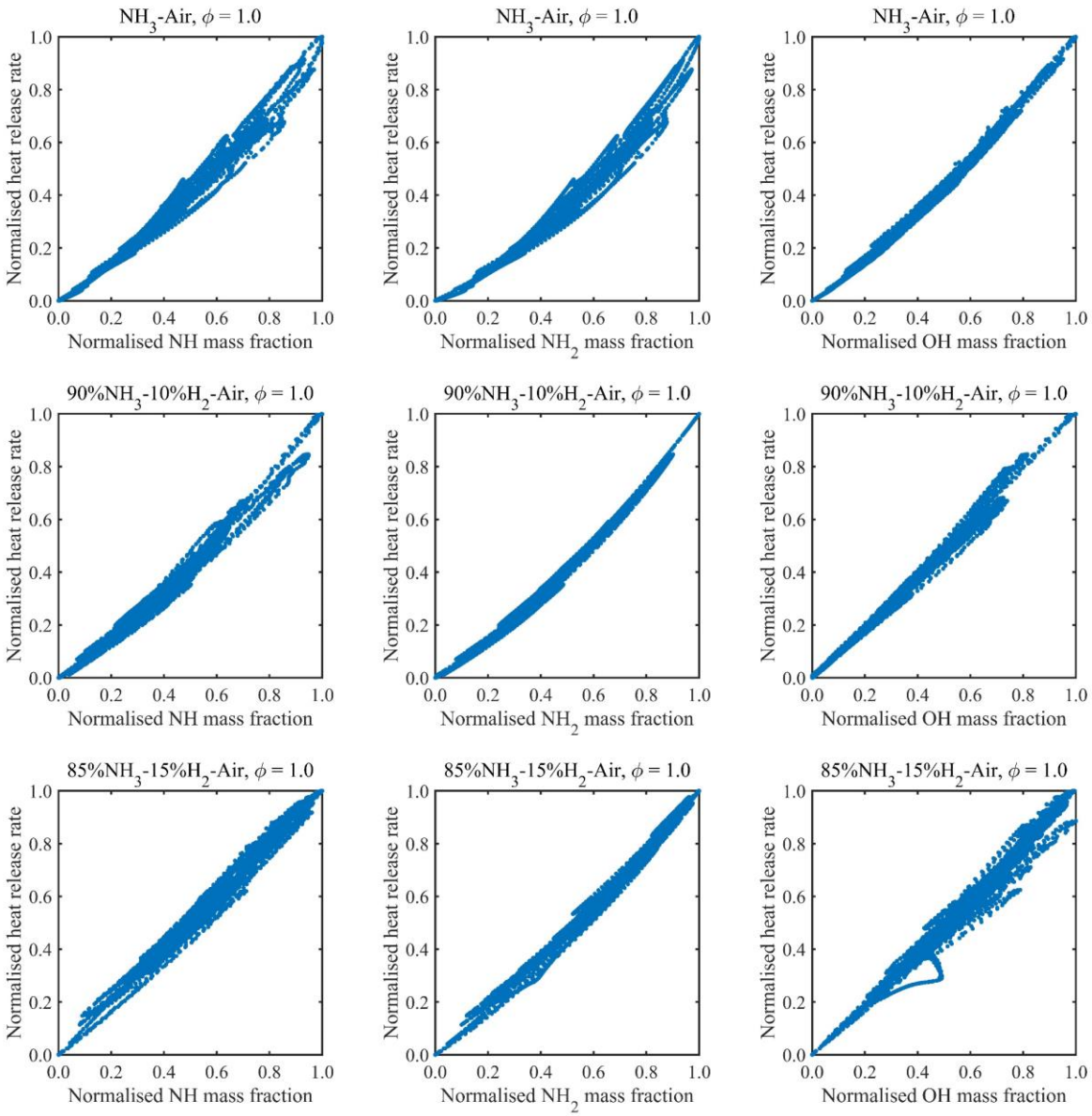

Fig.11. Scatter plots of normalised heat release versus normalised mass fraction of three radical species.

We analyse the relationship between radical species associated with ammonia combustion and heat release rate aiming to identify a possible flame maker for ammonia combustion. There is a research gap in identifying potential flame markers for ammonia combustion due to lack of exact measurements of radical species for ammonia combustion. Fig. 11 shows the normalised relationship between heat release rate and mass fraction of three radical species, NH, NH_2 and OH for ammonia and ammonia-hydrogen fuel blends at the stoichiometric condition. As seen

in Fig.11, the radical species NH_2 shows an excellent linear correlation with the heat release rate for the stoichiometric condition. Similar trends are observed for lean and rich conditions too. Furthermore, the radical species OH also shows a reasonable linear correlation with the heat release rate for the stoichiometric flame. Nevertheless, the DNS results suggest that NH_2 radical is more suitable to be considered as a heat release rate marker than OH radical for ammonia and ammonia-hydrogen fuel blends under spark-ignited premixed combustion mode. This should be further explored from the experimental investigation.

Burning velocity calculation

In this section, we study the burning velocities for all simulated test cases. The calculation is performed for all flames at mean flame radius, R=3.5mm. First, we study the laminar burning velocity and then discuss the turbulent burning velocity.

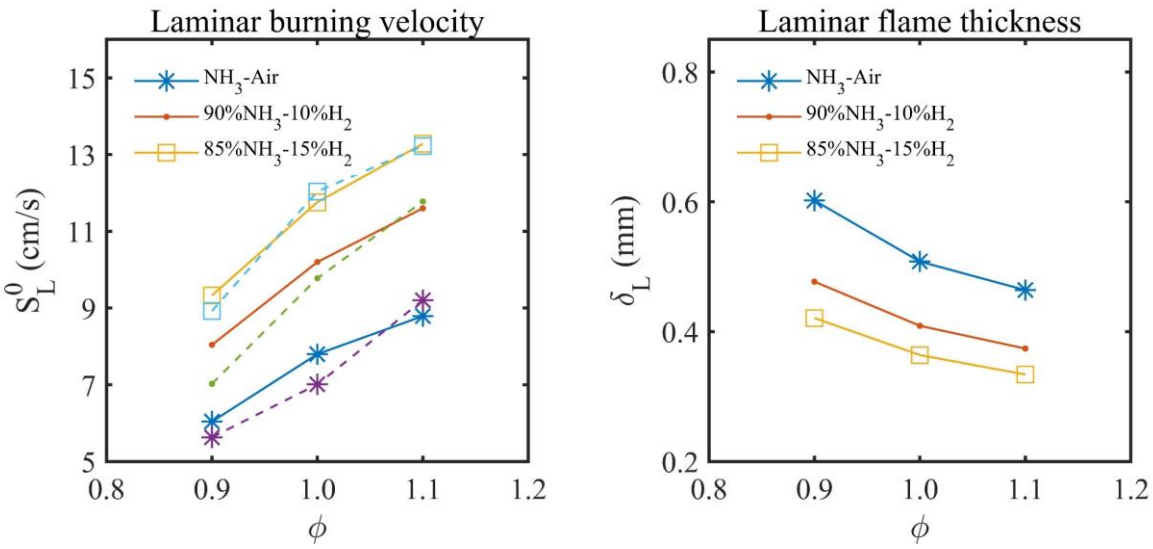

Fig. 12. Laminar burning velocity (left) and laminar flame thickness (right) as a function of equivance ratio for all test cases.

We have calculated laminar burning velocity and laminar flame thickness for all test cases using Cantera under the same temperature and pressure conditions and using the same

mechanism applied in DNS code, PARCOMB. Fig. 12 illustrates the laminar burning velocity for three fuel mixtures at lean, stoichiometric and rich conditions. The solid lines are the results based on Cantera while the dashed lines are the data from reference [46], in which the data derived from the experimentally tested spherical flame under laminar conditions. As seen in Fig. 12, simulated results show good agreement with the experimental data suggests that the chemistry mechanism we employed in our DNS study is sufficiently accurate to capture the burning characteristics of ammonia and ammonia-hydrogen blends at elevated pressures. As seen in Fig. 12, the laminar flame thickness is decreasing with respect to hydrogen addition for lean, stoichiometric and rich conditions, which shows the opposite trend compared to laminar burning velocity for all cases.

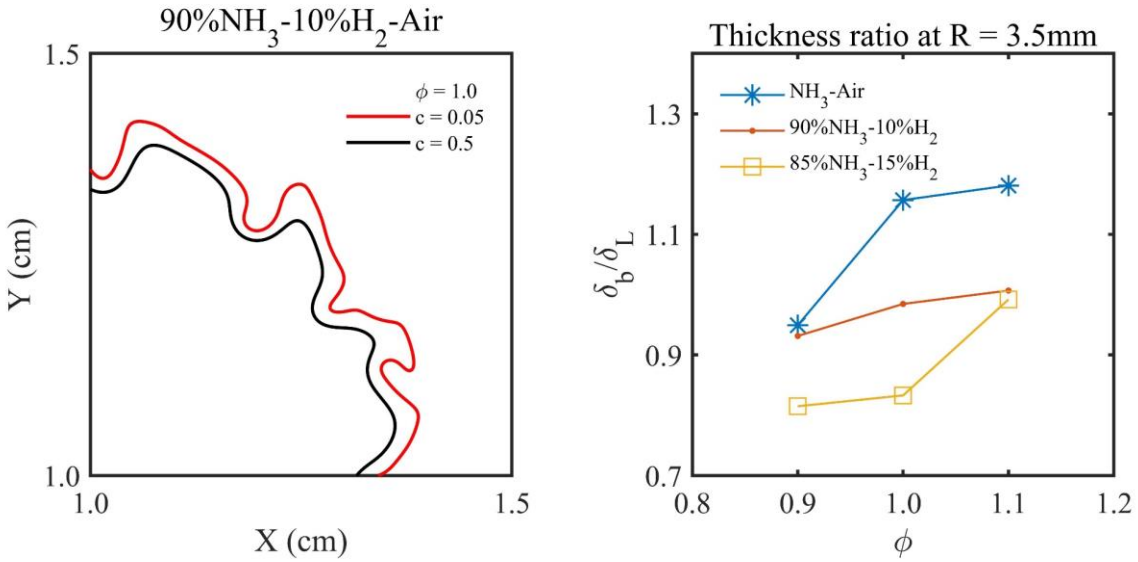

Fig.13. Example of mean progress variable (c) showing flame front, C = 0.5 and C = 0.05 (left) and flame brush ratio (right) as a function of equivalence ratio.

Fig. 13 shows contour plots of mean progress variable for one of the test cases to demonstrate how we calculated the turbulent flame brush thickness for all cases. As clearly seen in Fig. 13 (zoom view), two progress variables (c = 0.5 and 0.05) are chosen and then conducted two flame mean radius, of which difference is employed as the flame brush thickness. Fig. 13 also illustrates the ratio between the brush thickness and laminar flame thickness for all test cases. The pure ammonia flame exhibits high value for this ratio for all three equivalence ratios, showing the quick increase from lean to stoichiometric conditions and then slow change to rich condition. On the other hand, 10% hydrogen addition case exhibits much gentle variation for this ratio. This could be attributed to small distribution of convex and concave structures along the flame front.

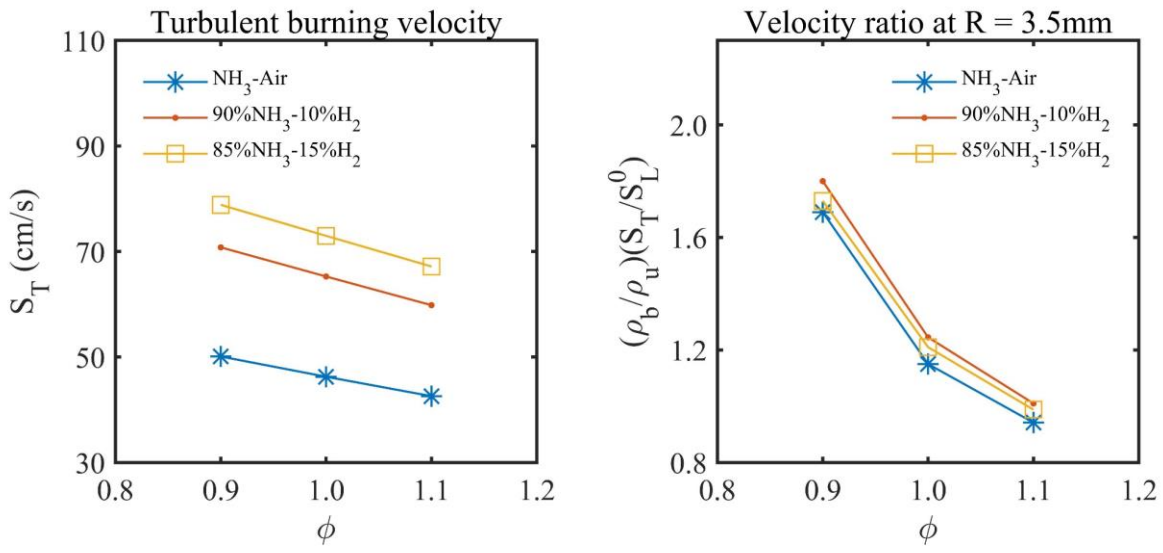

Fig.14. Turbulent burning velocity (left) and velocity ratio (right) as a function of equivalence ratio.

Fig. 14 shows the turbulent burning velocity at mean flame radius, R=3.5 mm by using the mathematical expression, $S_T = dR/dt$. The trend of turbulent burning velocity is decreasing with an increasing equivalence ratio for all test cases. The maximum value of S_T locates at the lean condition with equivalence ratio = 0.9. This trend has been observed in the experimental investigation for pure ammonia and ammonia-hydrogen fuel blends under high turbulence and

elevated pressure conditions [46]. This phenomenon means that the enhancement from high turbulent intensity has greater influence on the fuel lean condition instead of stoichiometric and fuel-rich conditions. This could happen due to strong flame front wrinkling in lean flames which enhances the fuel burning process and increases the turbulent burning velocity. Furthermore, Fig. 14 also shows increase in turbulent burning velocity with respect to more hydrogen addition into ammonia fuel at the same equivalence ratio. This could be attributed to the increasing trend for the effective Lewis number, which is most likely due to the effect of diffusional- thermal instability [55]. In general, high turbulent intensity and lower effective Lewis number (Le < 1, higher diffusion-thermal instability) would enhance the growth of flame surface area and increase the turbulent burning velocity.

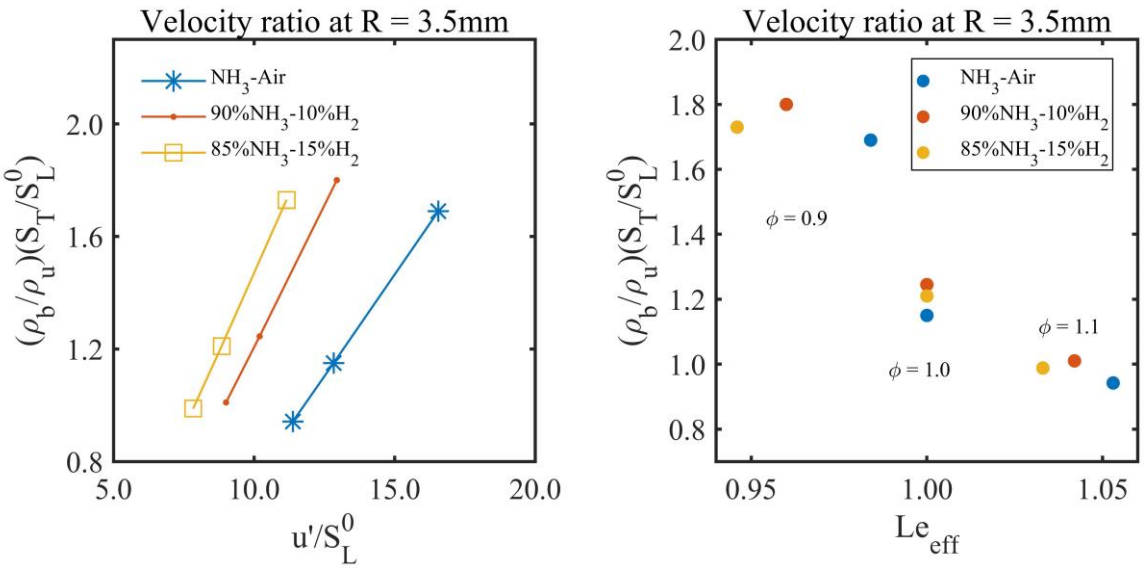

Fig. 15. The ratio of turbulent burning velocity to laminar burning velocity as a function of turbulence intensity (left) and effective Lewis number (right).

Fig. 15 illustrates the ratio of turbulent burning velocity to laminar burning velocity with different x-axis, named, turbulent intensity to laminar burning velocity and effective Lewis number. These result plots indicate that the maximum ratio occurs for 10% hydrogen addition case, not for 15% hydrogen addition case. This bending effect appears at all three equivalence ratios. This important trend with respect to ratio between turbulent to laminar burning velocity

has been identified by the experimental study in [46], but only for the lean condition with equivalence ratio 0.9. However, we have carried out additional test cases covering stoichiometric and rich conditions and we observed similar trends at lean, stoichiometric and rich conditions.

NO formation in flame structures

Even though there is no carbon emission in ammonia combustion, NOx formation cannot be ignored when combusting ammonia fuel with air. The issue is equally important for ammonia-hydrogen blends as blending hydrogen with ammonia would affect NOx formation. Different equivalence ratios would also make a great significance on NOx formation. This section will study the formation and local distribution of NO emission for the simulated flames at mean flame radius, R=3.5mm. Priority is given to identify how NO emission is formed in the small flame structures, including concave and convex structures in the reaction zone, which influence the distribution of NO.

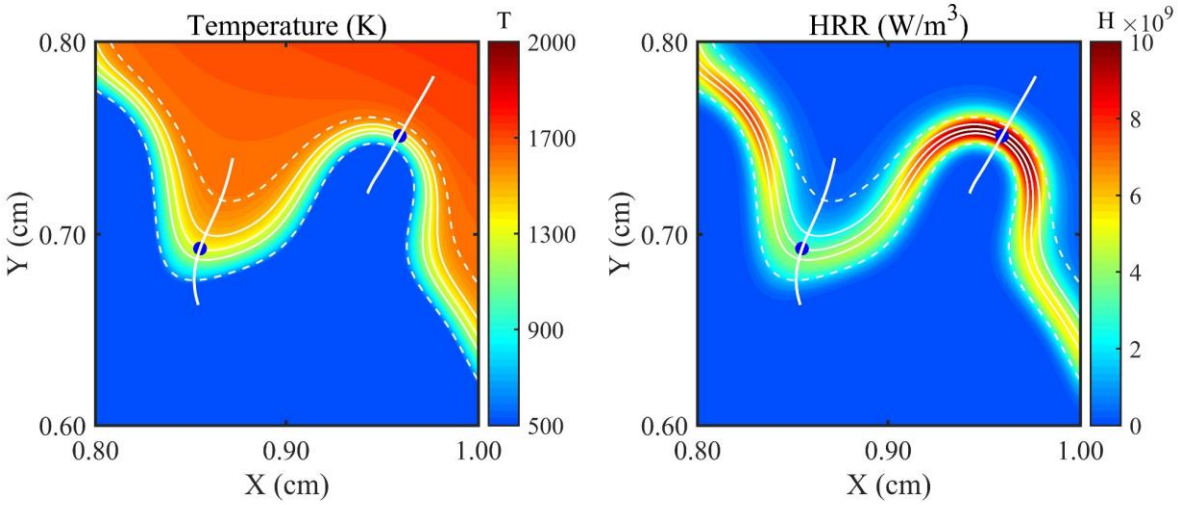

Fig. 16. Example contour for zoom view of the flame front including convex and concave structures: Temperature (left) and Heat release rate (right).

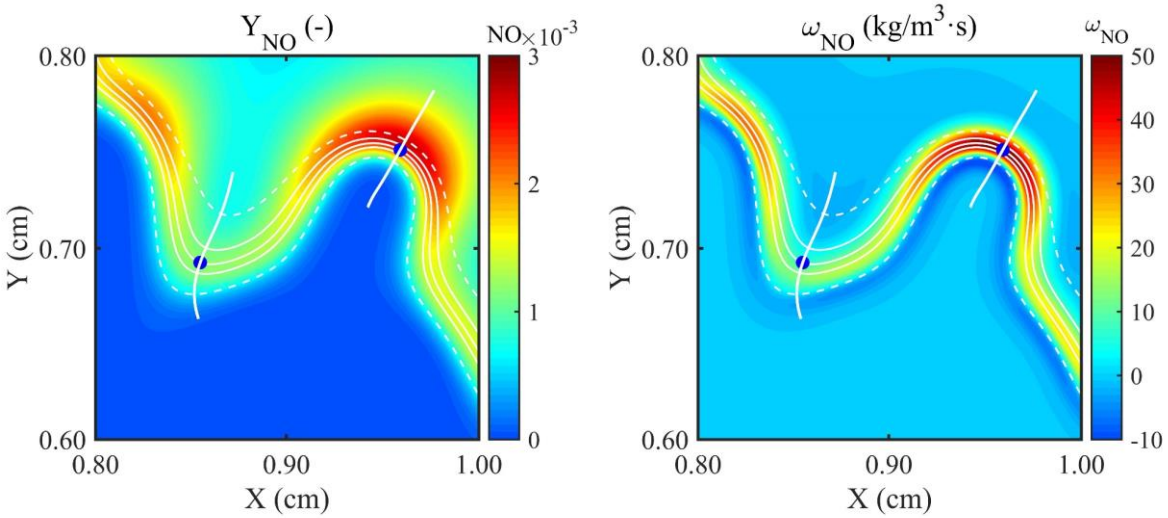

Fig. 17. Example contour for zoom view of the flame front including convex and concave structures: Mass fraction of NO (left) and NO reaction rate (right).

We will begin this section by analysing the relationship between the local heat release rate and local NO distribution. Fig. 16 shows the zoom view of temperature and heat release rate contour, herein ammonia-hydrogen test case with 10% hydrogen addition at stoichiometric condition is selected as an example. The blue region is in the unburned side and the red is in the burned side. Five lines are drawn in all contours, including the bottom dashed line representing the pre-heat zone (C = 0.1), three solid lines from bottom to top, representing the reaction layer, (C = 0.4, C = 0.5, C = 0.6) and the top dashed line representing the fully burned zone (C = 0.7). The peak heat release rate region is located at the flame front, C = 0.5, see Fig. 16 (right hand side). Two dots are selected on the flame front (C = 0.5) to show locations of the maximum and minimum heat release rate values respectively. The first dot is the maximum value of heat release rate along the flame front, which is located in the concave structure, and the second dot is the minimum value of heat release rate, which is located in the convex structure. The distribution of heat release rate is closely linked to the two distinct local flame

structures. Further, two lines are drawn to extract specific parameters, which are normal to the flame front and going through the pre-heat zone to fully burning region. To illustrate the relationship between local heat release rate and local NO formation, we study the mass fraction and reaction rate of NO in the same region as Fig.16 for the same test case. Fig. 17 shows the local distribution of mass fraction and reaction rate of NO. Apparently, the area of NO reaction rate is basically the same as the heat release rate. The main part of NO formation is occurring at the concave structure, which is consistent with the scattered plots presented in Figs. 7-10.

In order to understand the inter-dependency between NO formation and radical species along the flame front, we analyse the local equivalence ratio based on element of N and H with O. The local equivalence ratio based on the element of N, O and H, O are calculated by following equation:

$$\phi_{local} = \frac{Z_i/Z_O}{(Z_{i,u}/Z_{O,u})_{st}} \quad (8)$$

and

$$Z_i = \sum_{j=1}^{S} \mu_{ij} Y_j \quad (9)$$

where i means the considered element of N or H, S the total number of species, j the species and μij the mass proportion of i in j. Hence, the local equivalence ratio influences the local flame structure and the reaction of NO formation, resulting in the growth of the flame area.

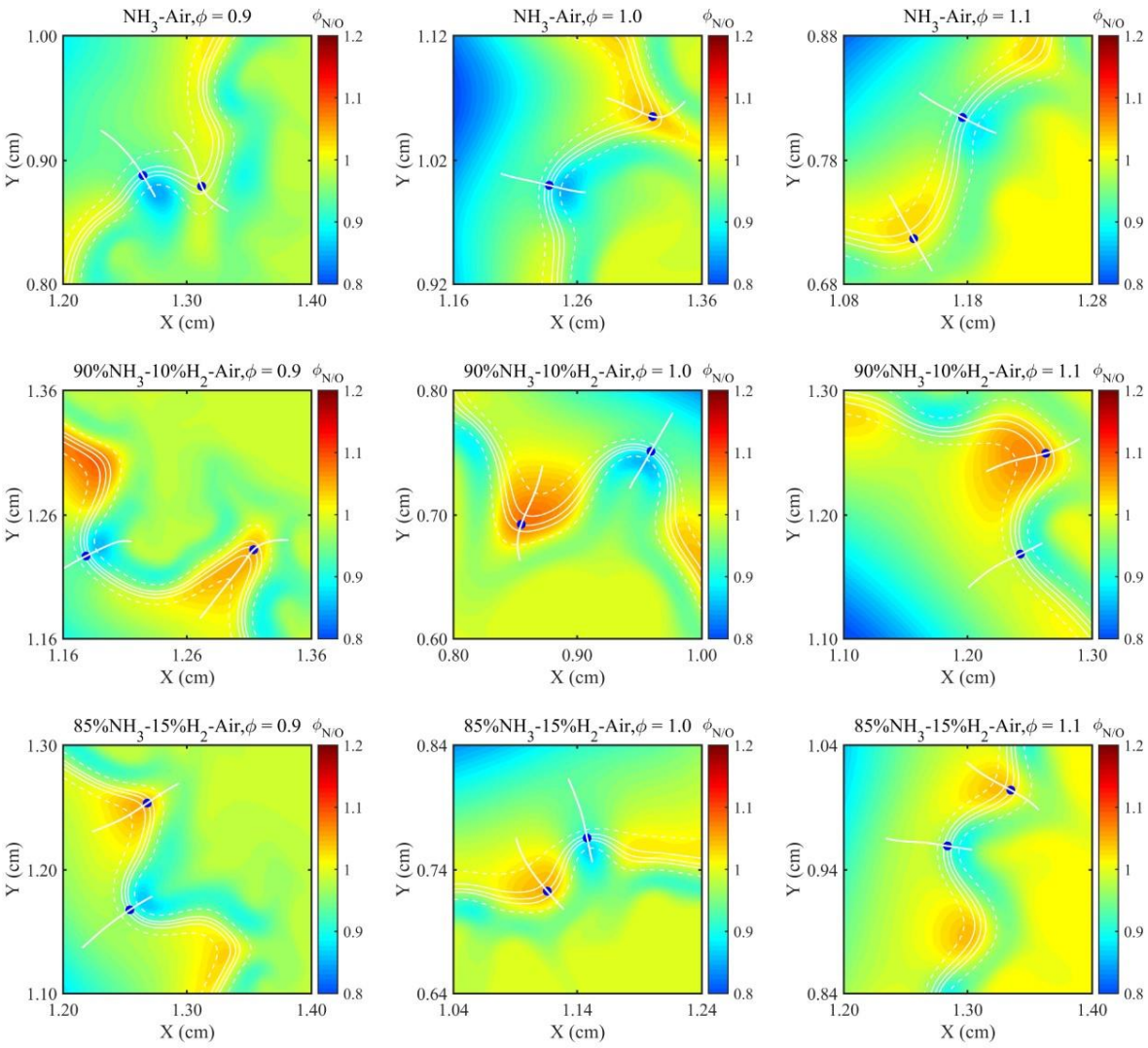

Fig. 18. Contours for zoom view of the flame front including convex and concave structures and local equivalence ratio, $\varphi_{N/O}$ for all flames.

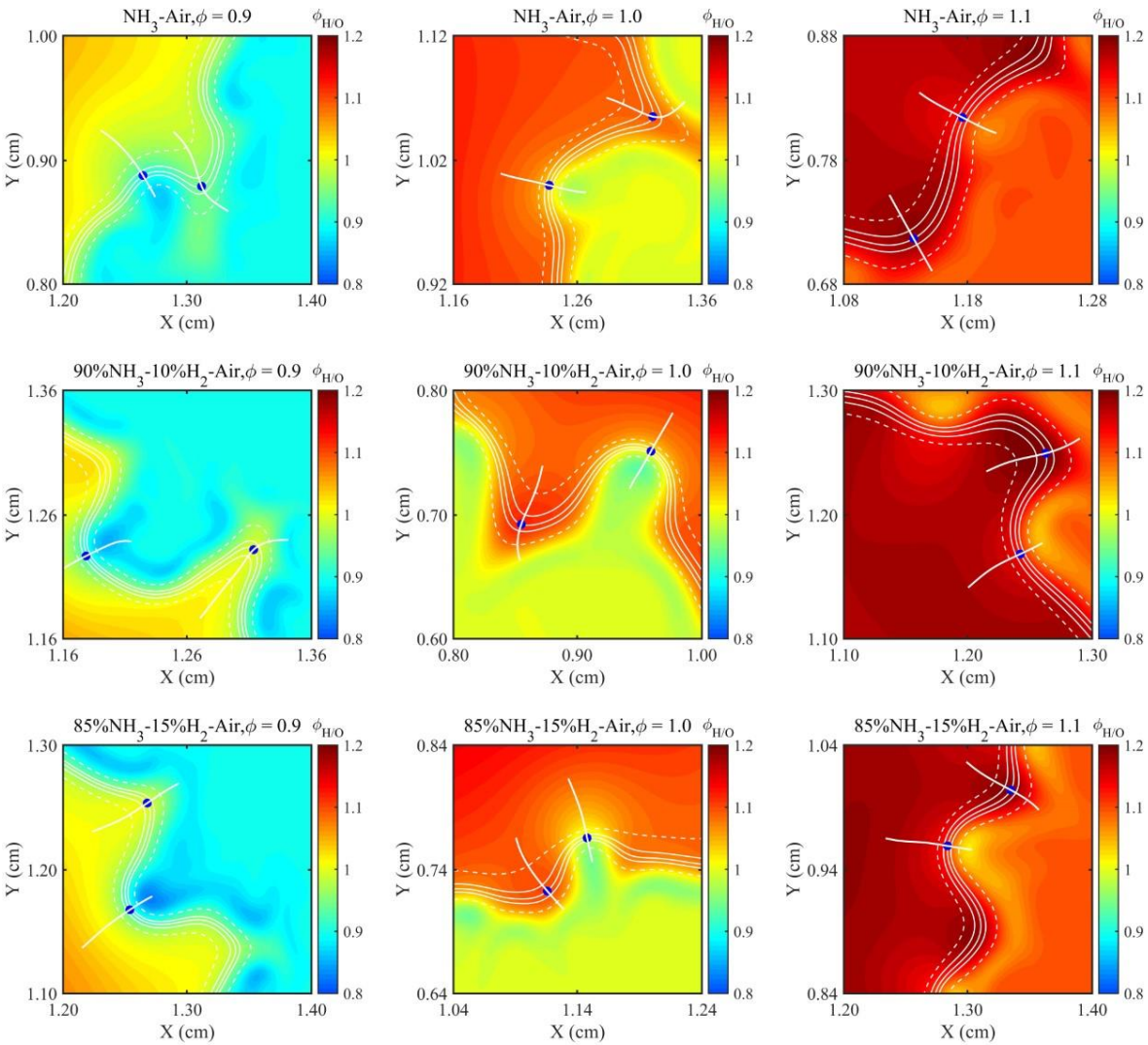

Fig. 19. Contours for zoom view of the flame front including convex and concave structures and local equivalence ratio, $\varphi_{H/O}$ for all flames.

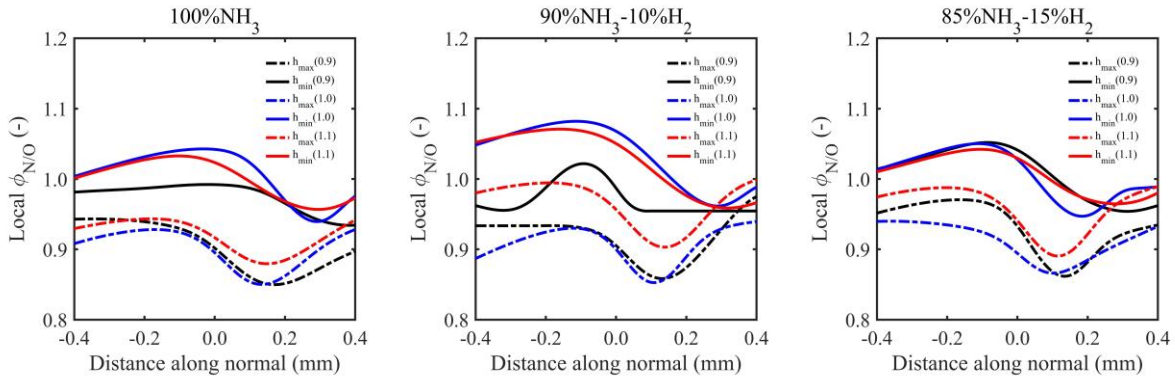

Fig. 20. Local equivalence ratio $\varphi_{N/O}$ at concave (dashed line) and convex (solid line) for three global equivalence ratios, 0.9 (black), 1.0 (blue), 1.1 (red).

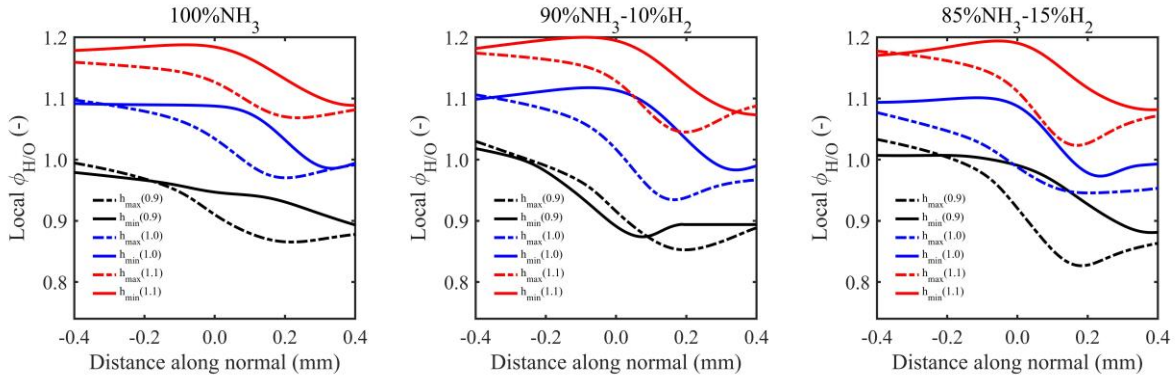

Fig. 21. Local equivalence ratio $\varphi_{H/O}$ at concave (dashed line) and convex (solid line) for three global equivalence ratios, 0.9 (black), 1.0 (blue), 1.1 (red).

Figs. 18 and 19 illustrate the distinct features of local equivalence ratio based on elements of N, O and H, O. Both Fig. 18 and Fig.19 show regional disparities appeared in concave and convex structures. It can be seen that the local equivalence ratio, $\varphi_{N/O}$, is not influenced by the global equivalence ratio and hydrogen addition, while showing apparent difference between concave (locally lean) and convex (locally rich) structures. This distribution is corresponding to the NO formation in the two distinct flame structures. Meanwhile, the local equivalence ratio, $\varphi_{N/O}$, is much sensitive to the global equivalence ratio rather than hydrogen addition. There is an obvious boundary on the both sides of the flame front. Fig. 20 and 21 illustrate the tendency of local equivalence ratio in the lines normal to the flame front for all nine simulated fuels.

Here, the positive values stand for the region ahead of the flame front, and negative values mean the downstream of flame while zero point is the dot which possess the maximum or minimum heat release rate. The two local equivalence ratios exhibit the decreasing and then increasing process from ahead (positive distance) to downstream (negative distance) of the flame front at the concave structure, accompanied with highest heat release rate.

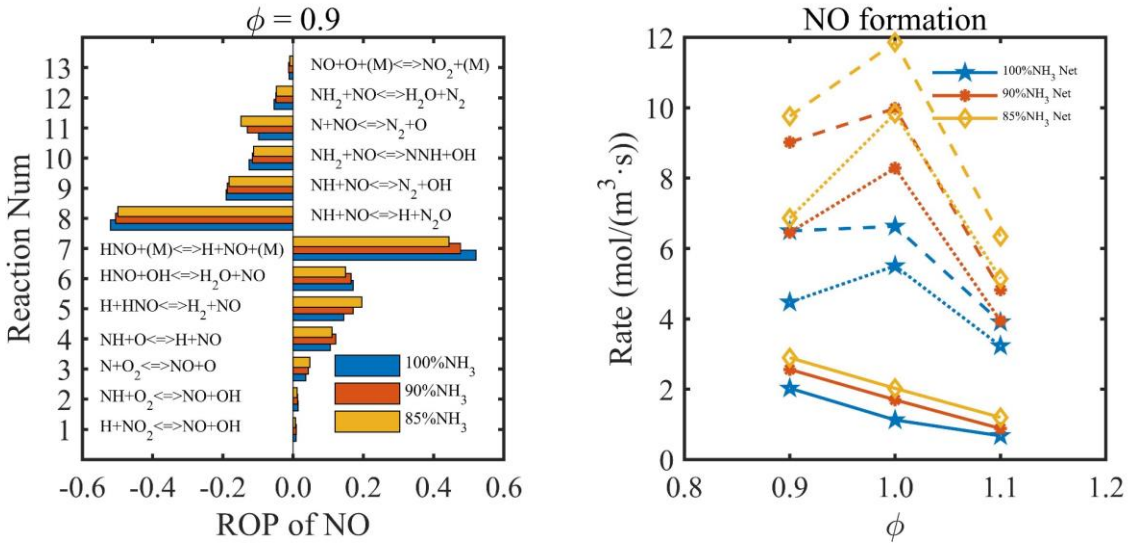

Fig. 22. ROP of maximum NO formation (left-hand side), and NO formation rate (right-hand side) for ammonia and ammonia-hydrogen flames at φ = 0.9. The NO formation rate is presented as production rate (dashed line), consumption rate (dot line), net reaction rate (solid line).

Finally, we performed the rate of production (ROP) analysis of NO formation at equivalence ratio, 0.9 and illustrate the NO formation rate in terms of production rate, consumption rate and net reaction rate in Fig. 22. Based on the chemistry mechanism we employed in our DNS calculation, 13 elementary reactions are involved in the production and consumption of NO. The results demonstrate that the addition of hydrogen into ammonia increases the NO formation. Both the production and consumption rate are enhanced by addition of hydrogen and the net reaction rate too is promoted by hydrogen addition which increases the NO formation. In the part of ROP, reaction 7 and reaction 8 are the main production and

consumption of NO, respectively. Even though the pure ammonia flame displays higher coefficients of ROP for reaction 7 and reaction 8, the percentage of both R7 and R8 are declining with more hydrogen addition, while other elementary reactions, such as R5 is increasing, which means these reactions may be the major source of higher NO formation with respect to hydrogen addition, and they become more reactive with more radical H production decomposition due to more hydrogen in the blended fuel mixture.

4. Conclusions

Direct numerical simulations on the study of outwardly expanding turbulent premixed spherical flames for ammonia and ammonia-hydrogen fuel blends with 10% and 15% hydrogen addition by volume at different equivalence ratios (0.9, 1.0, 1.1) under high turbulent intensity and elevated pressures were conducted to investigate the combustion characteristics under spark ignited engine-relevant conditions (445 K and 0.54 MPa). A detailed ammonia chemistry mechanism consists of 21 chemical species and 49 elementary reactions was employed for the simulations. Detailed mixture-averaged transport models (non-unity Lewis number model) with Soret effects were utilised to compute the diffusive processes.

The principal conclusions are as follows:

1. The analysis carried out in this study based on turbulent burning velocity and steady state NO production has found that outwardly expanding turbulent premixed spherical flames simulated in our DNS are fully developed. The contour plots of flame temperature, probability density distribution of the local curvature along the flame front reveal that the spherical flame front shows less wrinkled structures in fuel-rich flames compared to fuel-lean flames for pure ammonia and ammonia-hydrogen fuel blends.

2. Heat release rate distributions and the local curvature along the flame front illustrate distinct features between pure ammonia and ammonia-hydrogen flames. More hydrogen addition into

ammonia shows a higher heat release rate value which enhances the combustion intensity. For pure ammonia as well as ammonia-hydrogen blends, high values of heat release rate occurred in the region of concave structures (negative local curvature) and low values located in the region of convex structures (positive local curvature). The shift phenomena, the scattered distribution of heat release rate and local curvature reaching to zero curvature line, from pre-heat to fully burning region are observed, mainly occurring at the concave structures. This could be explained by the decreasing effective Lewis number, which quantified the thermal-diffusional instability.

3.With more hydrogen addition, the NO formation are significantly promoted, consistent with the higher values of heat release rate. The radical species of NH_2 has been identified as a potential heat release rate marker for ammonia and ammonia-hydrogen premixed combustion.

4. The hydrogen addition into ammonia increases the turbulent burning velocity. The highest turbulent burning velocity occurs at fuel-lean conditions for ammonia and ammonia-hydrogen fuel blends. This could be caused by the interaction of turbulence and thermal-diffusional instability with the presence of more wrinkled flame fronts. The ratio of turbulent burning velocity to laminar burning velocity indicates bending effects when changing fuel-air mixture from fuel-lean condition to fuel-rich condition. The ratio of turbulent flame brush thickness to laminar flame brush thickness shows distinct trends for all three flames with more gentle variation for ammonia-hydrogen fuel blend with10% hydrogen addition. The analyses of flame front behaviour, the ratio of turbulent to laminar burning velocity and the ratio of turbulent flame brush thickness to laminar flame thickness indicate that the optimum hydrogen addition of 10% by volume into ammonia provides the best burning characteristics for the expanding spherical turbulent premixed flame at high turbulence and elevated pressure.

5. NO formation at two distinct structures (concave and convex) are analysed by the combination of the elements (H, O and N), exhibiting higher NO emission at lower local

equivalence ratio. These two local equivalence ratios distinguish two different structures very well, lower region representing the concave structure related to higher NO formation and higher region on behalf of the convex structure related to lower NO formation.

6. Generally, both production and consumption rates of NO are intensified by the hydrogen addition into ammonia which resulted in higher net reaction rate. In perspective of ROP for three different fuels, the major sources of production (R7) and consumption (R8) are becoming less important with hydrogen addition, while other elementary reaction (R5) for NO production are gaining in proportion due to the increased reactivity of element H from the decomposition of hydrogen addition.

Acknowledgement

K. H. Luo gratefully acknowledges funding for the research and supercomputing time on ARCHER provided by the UK Engineering and Physical Sciences Research Council (EPSRC) under Grant Nos. EP/S012559/1 and EP/R029598/1.

References:

[1] Kobayashi H, Hayakawa A, Somarathne KDKA, Okafor EC. Science and technology of ammonia combustion. Proceedings of the Combustion Institute 2019;37:109-33.

[2] Valera-Medina A, Xiao H, Owen-Jones M, David WIF, Bowen PJ. Ammonia for power. Progress in Energy and Combustion Science 2018;69:63–102.

[3] Miller JA, Bowman CT. Mechanism and modeling of nitrogen chemistry in combustion. Progress in Energy and Combustion Science 1989;15:287–338.

[4] Konnov AA. Implementation of the NCN pathway of prompt-NO formation in the detailed reaction mechanism. Combust and Flame 2009;156:2093–105.

[5] Mendiara T, Glarborg P. Ammonia chemistry in oxy-fuel combustion of methane. Combust and Flame 2009;156:1937–49.

[6] Tian Z, Li Y, Zhang L, Glarborg P, Qi F. An experimental and kinetic modeling study of premixed $NH_3/CH_4/O_2$/Ar flames at low pressure. Combust and Flame 2009;156:1413–26.

[7] Duynslaegher C, Jeanmart H, Vandooren J. Flame structure studies of premixed ammonia/hydrogen/oxygen/argon flames: Experimental and numerical investigation. Proceedings of the Combustion Institute 2009;32:1277-84

[8] Duynslaegher C, Jeanmart H, Vandooren J. Ammonia combustion at elevated pressure and temperature conditions. Fuel 2010;89:3540–5.

[9] Klippenstein SJ, Harding LB, Glarborg P, Miller JA. The role of NNH in NO formation and control. Combust and Flame 2011;158:774–89.

[10] Duynslaegher C, Contino F, Vandooren J, Jeanmart H. Modeling of ammonia combustion at low pressure. Combust and Flame 2012;159:2799–805.

[11] Mathieu O, Petersen EL. Experimental and modeling study on the high-temperature oxidation of ammonia and related NO_x chemistry. Combust and Flame 2015;162:554–70.

[12] Song Y, Hashemi H, Christensen JM, Zou C, Marshall P, Glarborg P. Ammonia oxidation at high pressure and intermediate temperatures. Fuel 2016;181:358–65.

[13] Nozari H, Karaca G, Tuncer O, Karabeyoglu A. Porous medium based burner for efficient and clean combustion of ammonia-hydrogen-air systems. Int J Hydrogen Energy 2017;42:14775–85.

[14] Xiao H, Valera-Medina A, Marsh R, Bowen Philip J. Numerical study assessing various ammonia/methane reaction models for use under gas turbine conditions. Fuel 2017;196:344-51.

[15] Xiao H, Valera-Medina A. Chemical Kinetic Mechanism Study on Premixed Combustion of Ammonia/Hydrogen Fuels for Gas Turbine Use. Journal of Engineering for Gas Turbines and Power 2017;139:081504-1.

[16] Shrestha KP, Seidel L, Zeuch T, Mauss F. Detailed kinetic mechanism for the oxidation of ammonia including the formation and reduction of nitrogen oxides. Energy & Fuels 2018;32:10202–17.

[17] Okafor EC, Naito Y, Colson S, Ichikawa A, Kudo T, Hayakawa A, et al. Experimental and numerical study of the laminar burning velocity of CH_4-NH_3-air premixed flames. Combust and Flame 2018;187:185–98.

[18] Otomo J, Koshi M, Mitsumori T, Iwasaki H, Yamada K. Chemical kinetic modeling of ammonia oxidation with improved reaction mechanism for ammonia/air and ammonia/hydrogen/air combustion. Int J Hydrogen Energy 2018;43:3004–14.

[19] Glarborg P, Miller JA, Ruscic B, Klippenstein SJ. Modeling nitrogen chemistry in combustion. Prog Energy Combust Sci 2018;67:31–68.

[20] Rocha RC, Costa M, Bai XS. Chemical kinetic modelling of ammonia/hydrogen/air ignition, premixed flame propagation and NO emission. Fuel 2019;246:24-33.

[21] Shrestha KP, Lhuillier C, Barbosa AA, Brequigny P, Contino F, Mounaim-Rousselle C, Seidel L, Mauss F. An experimental and modeling study of ammonia with enriched oxygen content and ammonia/hydrogen laminar flame speed at elevated pressure and temperature. Proceedings of the Combustion Institute 2021;38:2163-74.

[22] Goodwin DG, Moffat HK, Speth RL. Cantera: an object-oriented software toolkit for chemical kinetics, thermodynamics, and transport processes. http://www.cantera.org 2021, version 2.4.0.

[23] ANSYS Chemkin-Pro. https://www.ansys.com/products/fluids/ansys-chemkin-pro 2021.

[24] Henshaw FP, D'Andrea T, Mann KRC. Premixed ammonia-methane-air combustion. Combustion science and technology 2005;177:2151-70.

[25] Lee JH, Lee SI, Kwon OC. Effects of ammonia substitution on hydrogen/air flame propagation and emissions. Int J Hydrogen Energy 2010;35:11332-41.

[26] Kumar P, Meyer TR. Experimental and modeling study of chemical-kinetics mechanisms for H_2–NH_3–air mixtures in laminar premixed jet flames. Fuel 2013;108:166-76.

[27] Hatakawa A, Goto T, Mimoto R, Arakawa Y, Kudo T, Kobayashi H. Laminar burning velocity and Markstein length of ammonia/air premixed flames at various pressures. Fuel 2015;159:98-106

[28] Nakamura H, Hasegawa S. Combustion and ignition characteristics of ammonia/air mixtures in a micro flow reactor with a controlled temperature profile. Proceedings of the Combustion Institute 2017;36:4217-26.

[29] Mei B, Zhang X, Ma S, Cui M, Guo H, Cao Z, Li Y. Experimental and kinetic modeling investigation on the laminar flame propagation of ammonia under oxygen enrichment and elevated pressure conditions. Combustion and Flame 2019;210:236-46.

[30] Han X, Wang Z, Costa M, Sun Z, He Y, Cen K. Experimental and kinetic modeling study of laminar burning velocities of NH_3/air, NH_3/H_2/air, NH_3/CO/air and NH_3/CH_4/air premixed

flames. Combustion and Flame 2019;206:214-26.

[31] Pochet M, Dias V, Moreau B, Foucher F, Jeanmart H, Contino F. Experimental and numerical study, under LTC conditions, of ammonia ignition delay with and without hydrogen addition. Proceedings of the Combustion Institute 2019;37:621-29.

[32] Okafor E C, Naito Y, Colson S, Ichikawa A, Kudo T, Hayakawa A, Kobayashi H. Measurement and modelling of the laminar burning velocity of methane-ammonia-air flames at high pressures using a reduced reaction mechanism. Combustion and Flame 2019;204:162-75.

[33] Liu Q, Chen X, Huang J, Shen Y, Zhang Y, Liu Z. The characteristics of flame propagation in ammonia/oxygen mixtures. Journal of Hazardous Materials 2019;363:187-96.

[34] Lhuillier C, Brequigny P, Lamoureux N, Contino F, Mounaim-Rousselle C. Experimental investigation on laminar burning velocities of ammonia/hydrogen/air mixtures at elevated temperatures. Fuel 2020;263:116653.

[35] Wang D, Ji C, Wang Z, Wang S, Zhang T, Yang J. Measurement of oxy-ammonia laminar burning velocity at normal and elevated temperatures. Fuel 2020;279:118425.

[36] Somarathne KDKA, Hayakawa A, Kobayashi H. Numerical investigation on the combustion characteristics of turbulent premixed ammonia/air flames stabilized by a swirl burner. Journal of Fluid Science and Technology 2016;16:00126.

[37] Kurata O, Iki N, Matsunuma T, Inoue T, Tsujimura T, Furutani H, Kobayashi H, Hayakawa A. Performances and emission characteristics of NH_3–air and NH_3-CH_4–air combustion gas-turbine power generations. Proceedings of the Combustion Institute 2017;36:3351-59.

[38] Xiao H, Valera-Medina A, Bowen P, Dooley S. 3D simulation of ammonia combustion in a lean premixed swirl burner. Energy Procedia 2017;142:1294-99.

[39] Somarathne KDKA, Hatakeyama S, Hayakawa A, Kobayashi H. Numerical study of a low emission gas turbine like combustor for turbulent ammonia/air premixed swirl flames with a secondary air injection at high pressure. Int J Hydrogen Energy 2017;42:27388-99.

[40] Somarathne KDKA, Colson S, Hayakawa A, Kobayashi H. Modelling of ammonia/air non-premixed turbulent swirling flames in a gas turbine-like combustor at various pressures. Combustion Theory and Modelling 2018;22:1-25.

[41] Ichikawa A, Naito Y, Hayakawa A, Kudo T, Kobayashi H. Burning velocity and flame structure of CH_4/NH_3/air turbulent premixed flames at high pressure. Int J Hydrogen Energy 2019;44:6991-99.

[42] Ichimura R, Hadi K, Hashimoto N, Hayakawa A, Kobayashi H, Fujita O. Extinction limits of an ammonia/air flame propagating in a turbulent field. Fuel 2019;246:178-86.

[43] Valera-Medina A, Gutesa M, Xiao H, Pugh D, Giles A, Goktepe B, Marsh R, Bowen P. Premixed ammonia/hydrogen swirl combustion under rich fuel conditions for gas turbines operation. Int J Hydrogen Energy 2019;44:8615-26.

[44] Okafor EC, Somarathne KDKA, Hayakawa A, Kudo T, Kurata O, Iki N, Kobayashi H. Towards the development of an efficient low-NO_x ammonia combustor for a micro gas turbine. Proceedings of the Combustion Institute 2019;37:4597-606.

[45] Okafor EC, Somarathne KDKA, Ratthanan R, Hayakawa A, Kudo T, Kurata O, Iki N, Tsujimura T, Furutani H, Kobayashi H. Control of NO_x and other emissions in micro gas turbine combustors fuelled with mixtures of methane and ammonia. Combustion and Flame 2019;211:406-16.

[46] Lhuillier C, Brequigny P, Contino F, Mounaim-Rousselle C. Experimental investigation on ammonia combustion behavior in a spark-ignition engine by means of laminar and turbulent expanding flames. Proceedings of the Combustion Institute 2021;38:5859-68.

[47] Xia Y, Hashimoto G, Hadi K, Hashimoto N, Hayakawa A, Kobayashi H, Fujita O. Turbulent burning velocity of ammonia/oxygen/nitrogen premixed flame in O_2-enriched air condition. Fuel 2020;268:117383.

[48] Hayakawa A, Hirano Y, Okafor EC, Yamashita H, Kudo T, Kobayashi H. Experimental and numerical study of product gas characteristics of ammonia/air premixed laminar flames stabilized in a stagnation flow, Proceedings of the Combustion Institute 2021;38:2409-17.

[49] Westbrook CK, Mizobuchi Y, Poinsot TJ, Smith PJ, Warnatz J. Computational combustion. Proceedings of the Combustion Institute 2005;30:125-57.

[50] Chen JH. Petascale direct numerical simulation of turbulent combustion-fundamental insights towards predictive models. Proceedings of the Combustion Institute 2011;33:99-123.

[51] Gerlinger W, Schneider K, Bockhorn H. Numerical simulation of three-dimensional instabilities of spherical flame structures. Proceedings of Combustion Institute 2000;28:793-99.

[52] Echekki T, Chen JH. Direct numerical simulation of autoignition in non-homogeneous hydrogen-air mixtures. Combust and Flame 2003;134:169–91.

[53] Altantzis C, Frouzakis CE, Tomboulides AG, Boulouchos K. Direct numerical simulation of circular expanding premixed flames in a lean quiescent hydrogen-air mixture: Phenomenology and detailed flame front analysis. Combustion and flame 2015;162:331-44.

[54] Yao T, Yang WH, Luo KH. Direct numerical simulation study of hydrogen/air auto-ignition in turbulent mixing layer at elevated pressures. Computers & Fluids 2018;173:59-72.

[55] Ranga Dinesh KKJ, Shalaby H, Luo KH, van Oijen JA, Thévenin D. High hydrogen content syngas fuel burning in lean premixed spherical flames at elevated pressures: effects of preferential diffusion. Int J Hydrogen Energy 2016;41:18231-49.

[56] Ranga Dinesh KKJ, Shalaby H, Luo KH, van Oijen JA, Thévenin D. Effects of pressure on cellular flame structure of high hydrogen content lean premixed syngas spherical flames: a DNS study. Int J Hydrogen Energy 2016;41:21516-31.

[57] Ranga Dinesh KKJ, Shalaby H, Luo KH, van Oijen JA, Thévenin D. Heat release rate variations in high hydrogen content premixed syngas flames at elevated pressures: Effect of equivalence ratio. Int J Hydrogen Energy 2017;42:7029-44.

[58] Bansal G, Mascarenhas A, Chen JH. Direct numerical simulations of autoignition in stratified dimethyl-ether (DME)/air turbulent mixtures. Combustion and Flame 2015;162:688-702.

[59] Netzer C, Ahmed A, Gruber A, Lovas T. Curvature effects on NO formation in wrinkled laminar ammonia/hydrogen/nitrogen-air premixed flames. Combustion and Flame 2021;232:111520.

[60] Thévenin D, Behrendt F, Maas U, Przywara B, Warnatz J. Development of a parallel direct simulation code to investigate reactive flows. Computers and Fluids 1996;25:485–96.

Declaration of interests

☒ The authors declare that they have no known competing financial interests or personal relationships that could have appeared to influence the work reported in this paper.

☐The authors declare the following financial interests/personal relationships which may be considered as potential competing interests: